

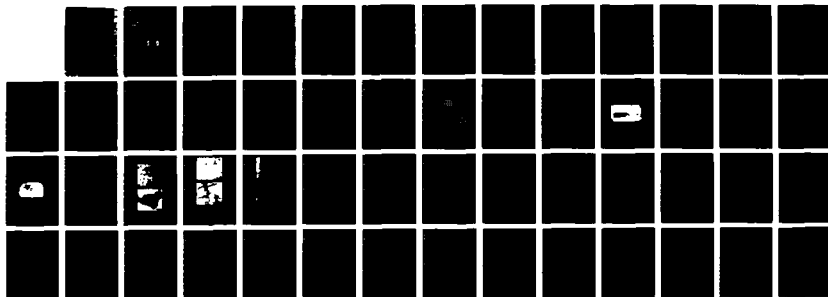
AO-A101 305

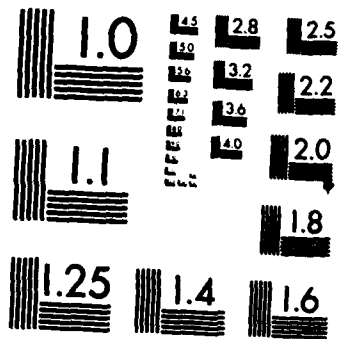
FUNDAMENTAL UNDERSTANDING OF THE INTRINSIC DUCTILITY IN
NICKEL-BASE L12 T. (U) PRATT AND WHITNEY WEST PALM
BEACH FL GOVERNMENT PRODUCTS DIV. . C C LAM ET AL.

1/1

UNCLASSIFIED

12 MAY 87 PM/GPD-FR-19001 AFOSR-TR-87-0771 F/G 11/6.1 NL





MICROCOPY RESOLUTION TEST CHART
NATIONAL BUREAU OF STANDARDS-1963-A

DTIC FILE COPY

②

AFOSR-TR-87-0771

FR 19801

AD-A181 385

FUNDAMENTAL UNDERSTANDING OF THE INTRINSIC DUCTILITY IN NICKEL-BASE L₁₂ TYPE ALLOYS

C.C. Law, D.M. Shah, J. Lin
United Technologies Corporation
Pratt & Whitney Group
Government Products Division
P.O. Box 2691
West Palm Beach, Florida 33402

Approved for public release;
distribution unlimited.

DTIC
ELECTE
S D
JUN 1 1 1987
CLD

12 May 1987

Annual Report
Period 15 February 1986 Through 14 February 1987

AIR FORCE OFFICE OF SCIENTIFIC RESEARCH (AFOSR)
NOTICE OF TRANSMITTAL TO DTIC
This technical report has been reviewed and is
approved for public release (AW AFR 150.12).
MATTHEW J. KEPPEL
Chief, Technical Information Division

Prepared for
Air Force Office of Scientific Research
Directorate of Electronic and Material Sciences
Building 410
Bolling AFB DC 20332-6448
Attn: Dr. Alan Rosenstein

AD-A181385

SECURITY CLASSIFICATION OF THIS PAGE

REPORT DOCUMENTATION PAGE

1a. REPORT SECURITY CLASSIFICATION Unclassified			1b. RESTRICTIVE MARKINGS			
2a. SECURITY CLASSIFICATION AUTHORITY AFOSR			3. DISTRIBUTION/AVAILABILITY OF REPORT AFOSR/DTIC			
2b. DECLASSIFICATION/DOWNGRADING SCHEDULE						
4. PERFORMING ORGANIZATION REPORT NUMBER(S) FR 19801			5. MONITORING ORGANIZATION REPORT NUMBER(S) AFOSR-TR 87-0771			
6a. NAME OF PERFORMING ORGANIZATION Pratt & Whitney		6b. OFFICE SYMBOL (If applicable) MERL		7a. NAME OF MONITORING ORGANIZATION Air Force Office of Scientific Research		
6c. ADDRESS (City, State and ZIP Code) United Technologies Corporation Pratt & Whitney Group Government Products Division Box 269 West Palm Beach, Florida 33402			7b. ADDRESS (City, State and ZIP Code) Directorate of Electronic and Material Sciences Building 410 Bolling AFB DC 20332-6448 Attention: Dr. Alan Rosenstein			
8a. NAME OF FUNDING/SPONSORING ORGANIZATION Air Force Office of Scientific Research		8b. OFFICE SYMBOL (If applicable) AFOSR		9. PROCUREMENT INSTRUMENT IDENTIFICATION NUMBER F49620-86-C-0033		
8c. ADDRESS (City, State and ZIP Code) Directorate of Electronic and Material Sciences Building 410 Bolling AFB DC 20332-6448 Attention: Dr. Alan Rosenstein			10. SOURCE OF FUNDING NOS.			
			PROGRAM ELEMENT NO.	PROJECT NO.	TASK NO.	WORK UNIT NO.
11. TITLE (Include Security Classification) Fundamental Understanding of the Intrinsic Ductility in Nickel-Base L12 Type Alloys						
12. PERSONAL AUTHOR(S) C. C. Law, D. M. Shah, J. Lin						
13a. TYPE OF REPORT Annual		13b. TIME COVERED FROM 2/15/86 TO 2/14/87		14. DATE OF REPORT (Yr., Mo., Day) 1987, 5, 12		15. PAGE COUNT 46
16. SUPPLEMENTARY NOTATION						
17. COSATI CODES			18. SUBJECT TERMS (Continue on reverse if necessary and identify by block number)			
FIELD	GROUP	SUB. GR.	Nickel Aluminide, Single Crystals, Ductility, Strength, ← Nickel alloys			
19. ABSTRACT (Continue on reverse if necessary and identify by block number)						
To study the effects of alloying on ductility of Ni3Al alloys, three series of alloys were formulated and produced as single crystals. The alloying additions selected include tantalum, tin and titanium which tend to destabilize the L12 lattice toward different derivative structures by changing the relative magnitudes of the planar fault energies. These alloying effects are being studied in terms of the structural configuration of dislocations produced, deformation behavior and the resulting ductility of the alloys. A major effort in the first year program was to grow single crystals of the selected alloys and some technical difficulties were encountered. Single crystals of all the selected alloys, with the exception of a tin-containing alloy have now been successfully grown. Tensile testing has been completed for a tantalum and a titanium-containing alloy. Relative to the binary alloy, the alloying additions were found to significantly increase the critical resolved shear strength CRSS for octahedral slip system without substantially affecting the CRSS for the cube slip system. A possible relationship between ductility of						
20. DISTRIBUTION/AVAILABILITY OF ABSTRACT UNCLASSIFIED/UNLIMITED <input checked="" type="checkbox"/> SAME AS RPT. <input type="checkbox"/> DTIC USERS <input type="checkbox"/>				21. ABSTRACT SECURITY CLASSIFICATION Unclassified		
22a. NAME OF RESPONSIBLE INDIVIDUAL C. C. Law			22b. TELEPHONE NUMBER (Include Area Code) Keyway (203) 565-1318		22c. OFFICE SYMBOL MERL	

19. Abstract (continued)

the alloys in polycrystalline form and the relative magnitudes of the CRSS for the two slip systems were discussed. Characterization of dislocations and deformation behavior in selected specimens tested is in progress.

TABLE OF CONTENTS

<u>Section</u>	<u>Page</u>
1.0 INTRODUCTION	1
1.1 Study Plan	3
1.1.1. Ductility Parameters	3
1.1.2. Alloy Formulation	4
1.1.3. Study of Deformation Behavior	4
2.0 EXPERIMENTAL	5
2.1 Preparation of Single Crystals	5
2.2 Mechanical Evaluation	5
2.3 Characterization of Microstructure and Deformation Behavior	6
3.0 RESULTS and DISCUSSION	6
3.1 Program Status	6
3.2 Characterization of Single Crystals and Microstructure	7
3.3 Tensile Test Results	9
4.0 SUMMARY	11
5.0 FUTURE WORK	12
6.0 REFERENCES	46



Accession For	
NTIS CRA&I	<input checked="" type="checkbox"/>
DTIC TAB	<input type="checkbox"/>
Unannounced	<input type="checkbox"/>
Justification	
By	
Distribution/	
Availability Codes	
Dist	Avail and/or Special
A-1	

LIST OF ILLUSTRATIONS

<u>Figure</u>	<u>Title</u>	<u>Page</u>
1	Schematic Diagram Summarizing the Effects of Various Solute Elements on Lattice Stability of the $L1_2$ Structure and the Likely Types of Dislocation Dissociation Which Would Occur. The Distribution of the Solute Atoms on the Close-Packed PLanes of Various Derivative Structures and Their Stacking Sequence are also Depicted	13
2	Schematic Drawing of Directional Solidification Process for Growth of Single Crystals	14
3	Drawing of Tensile Specimen Used for the Current Studies (Dimensions in Inches)	15
4	Appearance of a Single Crystal Ingot Removed From the Shell Mold	16
5	Distribution of $\langle 001 \rangle$ Directions on Various Locations on the Top and Bottom Faces of the Single Crystal Ingot of Alloy Al 240 With Reference to Three Orthogonal Axes Chosen to be Parallel to the Axis of the Ingot and the Dendrite Arm Directions	17
6	Distribution of $\langle 001 \rangle$ Directions on Various Locations on the Top and Bottom Faces of the Single Crystal Ingot of Alloy Ta 195 with Reference to Three Orthogonal Axis Chosen to be Parallel to the Axis of the Ingot and the Dendrite Arm Directions	18
7	Distribution of $\langle 001 \rangle$ Directions on Various Locations on the Top and Bottom Faces of the Single Crystal Ingot of Alloy Sn 204 with Reference to Three Orthogonal Axes Chosen to be Parallel to the Axis of the Ingot and the Dendrite Arm Direction	19
8	Appearance of a Crystal Section After Cylindrical Slugs with Different Crystallographic Orientations Have Been Removed by EDM Technique	20
9	Microstructure of Al 240 in the as-cast Condition. The Dark Phase is NiAl	21
10	Scanning Electron Micrograph of Sn 214 in the as-cast Condition. The Compositions of the Phases Labelled A, B and C in (b) are Given in Table 4	22

LIST OF ILLUSTRATIONS

<u>Figure</u>	<u>Title</u>	<u>Page</u>
11	Scanning Electron Micrograph of Sn 214 After a Heat Treatment of 50 Hours at 1339K. The Composition of the Phases Labelled A, B and C in (b) are Given in Table 4	23
12	Microstructure of Ta 225 Single Crystal (a) as-cast; (b) After 100 Hours at 1477K. The Dark Phase is NiAl	24
13	Average of the Actual Orientations for Tensile Specimens of Alloys Ta 195 (o) and Ti 1211 (o)	25
14	(a) Yield Strength Verses Temperature Curves of Single Crystal Specimens from Alloy Ta 195	26
14	(b) Yield Strength Verses Temperature Curves of Single Crystal Specimens from Alloy Ti 1211	27
15	Critical Resolved Shear Strength (CRSS) for Octahedral and Cube Slip Systems in Alloys Ta 195, Ti 1211 and Ni ₃ Al. The CRSS for Ni ₃ Al were Calculated from Data of Kear and Copley (Reference 6)	28
16	(a) Tensile Elongation Versus Temperature Curves for Alloy Ta 195	29
16	(b) Tensile Elongation Versus Temperature Curves for Alloy Ti 1211	30
17	Tensile Elongation Versus Temperature Curves for Alloys Ta 195, Ti 1211 and a Binary Ni ₃ Al Alloy (Reference 6) in <001> Orientation	31
18	A Comparison of Ratios of Critical Resolved Shear Strengths of Cube Slip to Octahedral Slip in Alloys Ta 195, Ti 1211 and a Binary Ni ₃ Al Alloy	32

LIST OF TABLES

<u>Table</u>	<u>Title</u>	<u>Page</u>
1	Nominal Compositions of Alloys Selected for the Study	33
2	Analyzed Alloy Compositions	34
3	Compositions of the Phases in Al 250 and Al 270	35
4	Compositions of the Phases in Sn 214 Single Crystal	36
5	Composition of the Phases in Ta 225 Single Crystal	37
6	Tensile Test Results for the Alloy Ta 195 (a) $\langle 001 \rangle$ Oriented Specimens	38
	Tensile Test Results for the Alloy Ta 195 (b) $\langle 011 \rangle$ Oriented Specimens	39
	Tensile Test Results for Alloy Ta 195 (c) $\langle 111 \rangle$ Oriented Specimens	40
	Tensile Test Results for Alloy Ta 195 (d) $\langle 123 \rangle$ Oriented Specimens	41
7	Tensile Test Results for Alloy Ti 1211 (a) $\langle 001 \rangle$ Oriented Specimens	42
	Tensile Test Results for Alloy Ti 1211 (b) $\langle 011 \rangle$ Oriented Specimens	43
	Tensile Test Results for Alloy Ti 1211 (c) $\langle 111 \rangle$ Oriented Specimens	44
	Tensile Test Results for Alloy Ti 1211 (d) $\langle 123 \rangle$ Oriented Specimens	45

SECTION 1.0

INTRODUCTION

The turbine section of a turbofan engine operates under the most extreme conditions. Stresses and temperatures are at high levels and compounded by the steep gradients and complex component geometries. Both turbine blades and disks demand the most advanced mechanical properties to sustain these operating conditions. Nickel superalloys have provided the required characteristics and the success of engines over the past twenty years can be traced in no small measure to the success of these alloys. However, new engines will be required to rotate faster and operate at higher temperatures to achieve the stretch performance goals that have been established. To reach these requirements, radically new approaches to alloy design are needed.

It is generally recognized that development of conventional nickel superalloys has reached a point of diminishing returns. One of the approaches to achieve property increases is to develop alloys based on intermetallic compounds. The approach is based upon the observation that the ordered structure of compounds often translate into superior high temperature properties. However, the options are severely restricted by ductility considerations for most of the high melting temperature intermetallic compounds are rather brittle at ambient temperatures. A necessary requirement for general plasticity is considered to be the operation of five independent slip systems. A candidate intermetallic, Ni_3Al , has an ordered fcc structure of the L1_2 -type, and deforms at low temperatures on $\{111\} \langle 110 \rangle$ slip systems which provides five independent slip systems. Not surprisingly, tensile ductility of Ni_3Al single crystals are very high, approaching 100% at room temperature (Reference 1).

However, Ni_3Al in polycrystalline form is brittle, failing at the grain boundaries with little or no plastic flow. The problem has been alleviated by the recent important discovery of the beneficial effect of boron microalloying on grain boundary cohesive strength of Ni_3Al (Reference 2) which has given impetus to several alloy development efforts based on this intermetallic. We and others have observed that the beneficial effects of boron, appear to be influenced significantly by alloy chemistry including stoichiometry, solute type and concentration. In particular, boron doped hyperstoichiometric Ni_3Al and dilute alloys ($\text{Al} + \text{Equivalent} > 25$ atomic percent) are brittle. Certain solutes, especially those which substitute for aluminum, also embrittle boron doped hypostoichiometric Ni_3Al when added in moderate quantities. The origin for the solute embrittling effects has been attributed entirely to unfavorable segregation behavior of boron in the presence of those solutes. Thus, a current approach to ductility problems in polycrystalline Ni_3Al alloys is through control of grain boundary chemistry by addition of various amounts of boron and related minor elements coupled with heat treatment control. This approach has been unsuccessful as evident from results of current Ni_3Al alloy development programs which show that no hyperstoichiometric alloys or ternary hypostoichiometric alloys containing moderate concentrations of certain solutes (titanium, for example) has yet been rendered ductile through manipulation of grain boundary chemistry.

A clue to some of the ductility problems in polycrystalline Ni₃Al alloys has been provided most recently from results of studies conducted at Pratt & Whitney indicating that, in contrast to the high ductility of the binary Ni₃Al single crystals (Reference 1), certain alloyed Ni₃Al single crystals can be quite brittle depending on specific alloy compositions and stoichiometry. For example, it has been observed that Ni₃(Al, Ti) single crystals containing 12 at/o Ti are so brittle that they cannot be machined without extensive cracking and hyperstoichiometric alloyed single crystals fracture in a brittle manner with low ductility. Obviously alloys which do not possess general plasticity in single crystal form will be rather brittle in polycrystalline form. An important implication from these observations is that the origin of some of the ductility problems in polycrystalline Ni₃Al alloys is due to a lack of intrinsic ductility in the grains/crystals, not weakness of grain boundaries per se. This realization could point to an important departure from our current approach which addresses the polycrystalline ductility problem entirely through control of grain size and grain boundary chemistry. It indicates a potentially fruitful area of research to provide insights into the effects of alloy composition on basic ductility/deformation and fracture behavior. We anticipate that as a result of the current studies, a set of guidelines will be developed for selection of alloys which are intrinsically ductile. These alloy compositional guidelines when coupled with the grain boundary strengthening with boron would provide a more logical basis for development of Ni₃Al alloys which are not only strong but are also ductile.

1.1 Study Plan

1.1.1 Ductility Parameters

The objective of this program is to provide insight into basic factors which control the intrinsic ductility of Ni_3Al alloys. The factors which are considered to be fundamentally important, and are being studied in this program, include the following:

Dislocation Characteristics - Fundamentally, plastic deformation is accomplished by generation and movement of dislocations through a crystal lattice. Thus, the intrinsic ductility of a crystal is governed by the ease with which dislocations are generated and the mobility of these dislocations. It can be shown analytically that both dislocation parameters are influenced by the configurational structure of the dislocations. Various types of configurational structures have been proposed depending on the planar fault energies in the ordered lattice.

The possible types of dislocation dissociations and their associated planar faults in the L1_2 lattice has been summarized recently by Pope and Ezz (Reference 1). Alloying can change the planar fault energies and favor one type of dislocation configurational structure over the other. For example, addition of Nb, Ta or V to Ni_3Al tends to reduce the antiphase boundary (APB) energy on $\{001\}$ planes and favor a simple configurational structure consisting of two superlattice dislocations connected by a strip of APB. The change in planar fault energies in a given lattice can also lead to instability of the lattice toward a derivative structure. For example, the addition of Nb, Ta or V in sufficient quantities can destabilize the L1_2 lattice toward D0_{22} lattice. These alloying effects on dislocation configurational structure and lattice stability has also been discussed by Pope and Ezz (Reference 1) and by Mishima, et al. (Reference 2) and schematically illustrated in Figure 1. As shown in Figure 1 that addition of Ni, Ta and Sn to nickel L1_2 alloys could theoretically lead to three different types of dislocation configurational structures. Therefore, it would be of interest to include tantalum-and tin-containing ternary alloys in our studies in order to establish experimentally a relationship between dislocation configurational structure and ductility.

Crystallography of Slip - In order for a crystal to be deformed to an arbitrary shape five independent slip systems must be available (Von Mises Criterion). This geometrical requirement may have an important consequence on ductility of L1_2 crystals. At low temperatures L1_2 crystals deform on octahedral slip systems $\{111\} \langle 110 \rangle$ which satisfy the Von Mises Criterion. However, at elevated temperatures slip on cube systems $\{100\} \langle 110 \rangle$ becomes important in L1_2 crystals. Shear deformation on the cube planes alone provides only three independent slip systems which are inadequate for accommodation of an arbitrary state of deformation as experienced, for example, by a grain in a polycrystalline aggregate or a single crystal deforming in a constrained manner as in a notch region. Therefore, primary cube slip could limit the ductility of L1_2 crystal at elevated temperatures. The temperature at which primary cube slip occurs in L1_2 crystals depends on orientation of the stress axis, the specific alloy composition and stoichiometry.

Structural Factors - Formation of localized lattice distortions associated with ordering of solute atoms at a sublattice could interfere with the mobility of dislocations due to coherency strain field around the distortions. The convergent beam electron diffraction technique (CBEB), which is extremely sensitive to localized lattice distortions, will be used to determine if such distortions are present in the alloys evaluated in these studies.

1.1.2 Alloy Formulation

The alloys selected for the present studies consist of three series, one binary series and two ternary series with tantalum and tin as the ternary additions which are kept constant at 5 atom percent and 4 atom percent, respectively. The variable within each series is the aluminum content which may have an important effect on ductility. In addition, a titanium containing Ni₃Al alloy with nominal composition of Ni, 12 atom percent Al and 11 atom percent Ti left over from a previous Pratt & Whitney program is also studied in the current program. Addition of Ti to Ni₃Al may lead to a dislocation configurational structure different from those due to alloying with Sn and Ta (Figure 1) since Ti tends to destabilize the L1₂ toward a different derivative (D024) lattice. Thus, inclusion of the titanium-containing alloy may provide a broader data base from which to construct a theoretical framework later in the program. The alloys are designated alphanumerically in which the ternary addition is indicated by alpha-bets followed by the concentrations of aluminum and the alloying addition, e.g. Sn 214 indicated a ternary Ni₃Al alloy consisting of 21 atom percent aluminum and 4 atom percent tin.

1.1.3 Study of Deformation Behavior

Single crystals were chosen to study deformation and fracture behavior of the alloys to provide the basic information required for quantitative analysis and modelling. Specimens are being tested with stress axes in <001>, <110>, <111> and <123> directions which are selected for the following effects:

- <001> No shear on the cube planes.
- <111> Near maximum shear stress on the cube planes and minimum shear stress on the octahedral planes.
- <123> Equal shear stress on cube and octahedral planes.

The slip behavior and fracture characteristics in the selection alloys are being studied using slip line observations and fractographic analysis. Transmission electron microscopy techniques are being used to characterize dislocation features in these alloys.

2.0 Experimental

2.1 Preparation of Single Crystals

Single crystals of alloys given in Table 1 were prepared using a modified Bridgeman crystal growth technique. About 9 kg (20 lb) of each alloy is melted in vacuum by induction heating using high purity elements as charge. The molten metal is then poured into a preheated ceramic shell mold with a helical crystal starter at the bottom which is in contact with a water-cooled copper chill. After pouring, the mold is slowly withdrawn from the furnace under conditions selected to promote growth of single crystal. The initial withdrawal rate was 76 mm/hour for 100 minutes after which the rate was increased to 102 mm/hour for the remainder of the crystal. Based on previous experiments, this technique typically results in crystals with $\langle 001 \rangle$ growth direction. A schematic diagram of the crystal growing system is given in Figure 2. More details of the directional solidification process for growth of single crystal may be found in Reference 3. The crystals produced for the current studies are 90 mm in diameter, 180 mm long. Such large crystals are necessary in order to have sufficient material for machining of tensile specimens with stress axes along various major crystal directions.

The single crystal ingots were centerless ground and macroetched to determine the presence of any undesirable secondary grains. Such grains, if present, were marked and the remaining single crystal further characterized using back reflection x-ray Laue diffraction technique. Because of the large dimensions (90 mm diameter, 180 mm long) of the crystals used in our studies, local variations in crystal orientation due to formation of subgrains are often encountered. To obtain an average orientation for the large crystals it is necessary to sample the crystal orientation at different locations on the bottom and top faces of the crystal. Typically five spots were electropolished at each end of the single crystal ingot and x-rayed along the axis of the ingot. Distribution of crystallographic orientations, as determined from the Laue results at various locations on the ingot were characterized with reference to three orthogonal directions, one of which is parallel to the axis of the ingot and the other two parallel to the dendrite arms. The specific crystallographic data from each ingot was then used to orient the ingot for machining of specimens with stress axes aligned along $\langle 001 \rangle$, $\langle 011 \rangle$, $\langle 111 \rangle$ and $\langle 123 \rangle$ as described in the next section.

2.2 Mechanical Evaluation

The ductility of the selected alloys is being evaluated using tensile testing. Special care was taken in the fabrication of tensile specimens from the single crystals, the sequence was as follows. First, cylindrical slugs about 10 mm diameter were wire EDM from the single crystal ingot at various angles calculated from the orientation of the ingot to yield cylinders of the selected orientations. The

specimen slugs were then solution heat treated for 100 hours at 1477K for the binary and the tantalum-containing ternary alloys, 1066C for the tin-containing alloys. Subsequently, the slugs were hot isostatically pressed (HIP) at the respective solution treatment temperature for 3 hours at 100 MPa. This treatment minimizes the amount of casting porosity in the crystals. The axial orientation of each slug was reconfirmed by x-ray analysis prior to machining of tensile specimens. Plate-type of tensile specimens with dimensions given in Figure 3 were then wire EDM from the HIP slugs. Testing of the specimens was conducted at 293K, 700K, 1033K and 1090K and flow and fracture stresses determined.

2.3 Characterization of Microstructure and Deformation Behavior

The microstructure of each of the alloys was determined using standard optical metallographic techniques. The composition of phases present in selected alloys were studied using a quantitative electron microprobe technique with elemental standards as references.

The deformation behavior was analyzed using both slip line observations and transmission electron microscopy techniques. Before testing specimens were mechanically polished and then electrochemically polished in a 15% H₂SO₄ in methanol solution at 20V and 293K. This provides a smooth surface that is necessary for slip trace observations. After deformation slip trace directions on two adjacent faces of the specimen were measured and analyzed to determine slip planes. For detailed TEM analysis 3 mm discs were taken from wafers cut parallel to slip planes as determined by slip trace analysis. The wafers were cut using a diamond saw. The foils were electropolished using a solution of 6% perchloric acid in equal parts of methanol, ethanol and butanol in a Fischione twin jet electropolisher operated at 30V, 7 ma/mm, and 258K.

Thin foils were also used to study localized lattice distortion due to substitutional ternary alloying additions. Convergent Beam electron diffraction (CBED) techniques were used. Characteristic triangle formed by {359} holz lines in the zero order central disc was generated for analysis from exactly {111} oriented foil samples. These holz lines which are very sensitive to variations in lattice parameter and crystal symmetry can be used to reveal subtle effects due to local ordering of substitutional solutes.

3.0 Results and Discussion:

3.1 Program Status

A major effort in the first year program was to produce single crystals of the nine selected alloys with compositions given in Table 1. Progress has been hampered by a major relocation of the Pratt & Whitney developmental foundry facility during the first year program. In addition several experimental problems have been encountered. Crystals of some alloys could be grown relatively easily while others

required several runs, each with a different combination of temperature and growth rate parameters, before high quality single crystals could be produced. At present, all the alloys, with the exception of alloys Al 250 and Sn 234, have been successfully grown. However, smaller crystals (25 mm diameter bars) of Al 250 have been produced and will be used for our study. Effort is continuing to produce Sn 234 in single crystal form.

Currently all the alloys that have been successfully grown into large single crystals are either in the final stage of specimen machining or are being tested. Testing has been completed for alloys Ta 195 and Ti 1211. Results are presented in the next section. Transmission electron microscopy is in progress.

3.2 Characterization of Single Crystal Orientation and Microstructure

The analyzed compositions of the single crystal ingots are given in Table 2 and show only minor deviations from the aim. The appearance of the single crystal ingot removed from the shell mold is shown in Figure 4. Examples of the distribution of crystal orientations determined on several locations from the top and bottom faces of the ingot using Laue diffraction technique, are illustrated in Figures 5, 6 and 7 in which the $\langle 001 \rangle$ directions from each location were plotted with reference to three orthogonal axes chosen to be parallel to the axis of the ingot and the dendrite arm directions. The average orientation of the $\langle 001 \rangle$ directions is indicated by square symbols in the plots. Figure 5 shows that the $\langle 001 \rangle$ growth direction of the Al 240 crystal is several degrees away from the axis of the ingot and that there is relatively little scatter in crystal orientations at various locations in the crystal. The orientation distribution plot for the Ta 195 single crystal, given in Figure 6, shows that $\langle 001 \rangle$ crystal growth direction is nearly parallel to the axis of the ingot but there is relatively large scatter in crystal orientations at various locations, compared with Al 240 (Figure 5). An example which shows both a large deviation of the $\langle 001 \rangle$ crystal growth direction from the ingot axis and relatively large scatter in crystal orientations is shown in Figure 7 for the Sn 204 single crystal. These average crystal orientation data were used to orient the ingot during extraction of cylindrical slugs with axes parallel to $\langle 001 \rangle$, $\langle 110 \rangle$, $\langle 111 \rangle$ and $\langle 123 \rangle$ directions using wire EDM technique, and a machined crystal is shown in Figure 8. The actual orientation of each slug was determined after heat treatment and used for subsequent analysis of data. Typically, the actual orientation was found to be within 10 degrees from the target orientation.

Ideally the alloys for ductility study should be single phase and free of segregations and casting defects. However, due to the solidification behavior of the alloys selected, a second phase was found in all the crystals in the as-cast condition. Thus, attempts are being made to minimize the amount of the second phase by heat treatment. In the absence of an ideal microstructure, it is important to characterize the amount of the second phase present in the alloys and the

partitioning behavior of aluminum and the ternary alloying addition among the phases. These microstructural and compositional data will be taken into consideration in subsequent analysis of the ductility data.

The microstructures of all the binary alloy single crystals in the as-cast condition consist of NiAl and Ni₃Al phases (Figure 9). The amount of the NiAl increases with increasing Al content and about 10 volume percent was observed in Al 270 in which the NiAl phase formed as dendrites. The phase compositions of alloys Al 250 and Al 270 were determined using electron microprobe techniques and the results are given in Table 3 which show that the Ni₃Al is slightly hypostoichiometric and hyperstoichiometric in alloys Al 250 and Al 270, respectively. Heat treatment studies on the binary alloys are being conducted in an attempt to reduce the amount of NiAl phase. The heat treatment conditions are based on a more accurate Ni-Al phase diagram kindly provided to us by Dimiduk (Reference 4).

The microstructure of the tin-containing Ni₃Al alloys appear rather similar. The differences seem to be primarily in the amount and distribution of the phases. Therefore, microstructure and electron microprobe results are presented for SN 214 only. Figure 10 shows scanning electron micrographs of the microstructure of Sn 214 single crystal in as-cast condition. The presence of three different phases, labelled A, B and C in Figure 10b, is apparent. Heat treating the alloy for 50 hours at 1339K produced no important changes in the microstructure (Figure 11) although the phase boundaries become more distinctive. As shown in Table 4 some changes in phase composition took place during heat treatment. Table 4 also shows that Phase A, the major constituent, is the ternary L1₂ phase Ni₃Al, phase B is probably a D019 phase Ni₃Sn with Al substituting at the Sn sublattice and Phase C is probably a B8 type compound Ni₃Sn₂, again with some substitution of Al at the Sn sublattice.

The microstructure of the tantalum-containing Ni₃Al alloys consist of Ni₃Al and NiAl phases. As expected, the amount of the NiAl phase increases with the aluminum content and reaches about 8 volume percent in alloy Ta 225 which contains the highest Al content. Both the microstructure and phase composition in the tantalum-containing alloys were found to be rather stable, only minor changes resulted from a heat treatment for 100 hours at 1477K (Figure 12). The compositions of the phases in alloy Ta 225 are shown in Table 5 which shows a much larger solubility for Ta in Ni₃Al, than in the NiAl phase. Further, if one assumes that all the Ta atoms occupy only the Al sublattice sites, than the L1₂ phase in Ta 225 is hyperstoichiometric. Stoichiometry has been shown to play a major role in the ductility of polycrystalline Ni₃Al alloys. The role of stoichiometry in basic deformation behavior will be a subject of our study in the near future.

3.3 Temperature and Orientation Dependence of Strengths and Ductility

A comparative study of the temperature dependence of plastic anisotropy of single crystal Ni_3Al alloys is considered crucial to a basic understanding of the ductility of this class of materials with $L1_2$ structure. To meet this objective, tensile specimens machined in the four major orientations $\langle 001 \rangle$, $\langle 011 \rangle$, $\langle 111 \rangle$ and $\langle 123 \rangle$ were tested between room temperature and 1144 K (1600F). Testing has been fully completed for two alloys Ta 195 and Ti 1211.

The tensile test results for the alloys Ta 195 and Ti 1211 are presented in Table 6(a)-(d) and Table 7(a)-(d) respectively. In each case the results for each of the four major orientations are presented in separate tables (a) to (d). The average of actual orientation of the top and bottom ends of the cylindrical slug from which multiple specimens were machined is also included for each specimen. The orientation is described in terms of three angles the specimen axis makes with respect to the principal $\langle 001 \rangle$ directions. The average of the actual orientations for the two alloys tested are plotted in a stereographic triangle in Figure 13 which show that all of the orientations are within 10 degrees from the aim. The largest scatter in orientations between the two alloys can be observed in $[123]$ and $[011]$. As will be shown these orientational differences may have resulted in apparent differences in ductility behavior between the two alloys in these two orientations. The axial orientation angles are used to calculate the appropriate Schmid factors for the primary octahedral and cube slip systems as shown in lower part of each table. These factors in turn are used to resolve the yield stress into shear strength components.

The tensile yield strengths are plotted against temperature in Figure 14a and b for the alloys Ta 195 and Ti 1211 respectively. Qualitatively it is apparent that the orientation and temperature dependence of yield strength of both the alloys is similar. In both alloys the most anomalous rise in strength with temperature is observed for the $\langle 001 \rangle$ orientation, as expected. Other orientations show yield strength peaks around 700K. In the $\langle 001 \rangle$ oriented specimens in which the resolved shear stress RSS for cube slip is insignificant the RSS for the octahedral slip can be considered a true indication of the critical resolved shear strength CRSS. There is no such clear way of assessing the CRSS of cube slip since there is no orientation for which the octahedral slip can be completely suppressed. Nevertheless, the behavior of $\langle 111 \rangle$ orientation is a good indication of the CRSS on cube slip since the orientation is geometrically better disposed to deform by cube slip than octahedral slip. Thus, it is quite logical to assume that the temperature region in which the RSS for cube slip based on the $\langle 111 \rangle$ orientation is significantly lower than the CRSS for octahedral slip based on $\langle 001 \rangle$ orientation, the material would deform predominantly by cube slip. From the yield strength data for $\langle 001 \rangle$ and $\langle 111 \rangle$ specimens and with some simplifying assumptions the CRSS for octahedral and cube slip can be calculated which are shown in Figure 15. The effect of constriction stress for

the Shockly partials as discussed by Lall et. al. (Reference 5) was not taken into consideration in the CRSS calculations. The CRSS for the binary Ni_3Al calculated from yield strength data of Kear and Copley (Reference 6) are also included in Figure 15 for comparison. Figure 15 shows interestingly that the CRSS for the cube slip in Ni_3Al are relatively unchanged by the tantalum or titanium additions. In contrast, the CRSS for octahedral slip in Ni_3Al are increased significantly by the alloying additions. An apparent consequence of these CRSS changes on ductility will be discussed in the following.

The tensile ductility of Alloys Ta 195 and Ti 1211 are given in Figure 16 which shows that ductility is determined significantly by crystal orientation and temperature. The ductility behavior of specimens with $\langle 001 \rangle$ and $\langle 111 \rangle$ orientations is rather similar for the two alloys. The fracture elongations of $\langle 001 \rangle$ specimens remain at 10 to 20% level, relatively unchanged by test temperature. The $\langle 111 \rangle$ specimens which have the lowest ductility at room temperature among all the orientations studied show rapid increase in ductility with temperature and reach a ductility peak at about 1100K. Since the two alloys presumably deformed by cube slip because of the lower CRSS for cube slip (Figure 15) in the temperature regime where significant ductility increase is observed, the $\langle 111 \rangle$ ductility data suggest that the mobility of dislocations in the cube slip systems is high at intermediate temperatures. In contrast to the $\langle 001 \rangle$ and $\langle 111 \rangle$ orientations there are some noticeable ductility differences between the two alloys in the nominally $\langle 011 \rangle$ and $\langle 123 \rangle$ orientations. The reasons for the observed differences are not clear at present, it could be due to differences in the specific orientations of the specimens (see Figure 13) or specific compositions of the alloys. The ductility trends as a function of alloy composition, orientation and temperature will be studied in greater detail in the near future as more data become available.

It is interesting to compare the tensile ductility of the two ternary alloys in $\langle 001 \rangle$ orientation with the binary alloy studied by Copley and Kear (Reference 6), Figure 17. The binary alloy shows significantly higher ductility at low temperatures compared with the ternary alloys, and the ductility decreases with increasing temperature to a minimum at about 1100K. The difference in ductility behavior between binary and the Alloys Ta 195 and Ti 1211 is related to the configurational structures of the dislocations present in these alloys. This aspect is being studied in this program using transmission electron microscopy technique. Since the configurational structure of dislocations is related to various planar fault energies which, in turn, would change the dislocation mobility on octahedral and cube slip systems, a correlation of CRSS for octahedral and cube slip with ductility is suggested. Indeed, if one plots the ratios of CRSS for cube slip to the CRSS for octahedral slip as a function of temperature for the binary alloy and the ternary alloys as a group, the curves follow the same trend as the $\langle 001 \rangle$ ductility curves, Figure 18. It becomes apparent that in general the smaller the ratio (more readily cube slip occurs) the lower the $\langle 001 \rangle$ ductility. In fact for the isostructural compound Pt_3Al for which the CRSS ratio is always less than unity, the alloy in $\langle 001 \rangle$ orientation has been found to be extremely brittle at low temperatures (Reference 7).

3.4 Ductility of Polycrystalline Ni₃Al Alloys

It has been shown that boron doped polycrystalline Ni₃Al alloys with compositions similar to those of Ta 195 and Ti 1211 show rather low ductility in the temperature range currently studied (Reference 8). In contrast, the boron doped polycrystalline binary alloy shows high ductility at room temperature and the ductility decreases with increasing temperature. Thus, qualitatively the ductility of the polycrystalline alloys and the ductility of single crystals in <001> orientation follow similar trends. The cause for the apparent similarities may be basically related to the fact that only octahedral slip can contribute toward ductility for both the polycrystalline alloys and the <001> crystals. As indicated in the last section, increasing the CRSS ratio for cube slip to octahedral slip may be an effective technique for improving ductility of polycrystalline Ni₃Al alloys. This aspect will be studied further as more data become available in this program.

4.0 Summary

To study the effects of alloying on ductility of Ni₃Al alloys, three series of alloys were formulated and produced as single crystals. The alloying additions selected include tantalum, tin and titanium which tend to destabilize the L1₂ lattice toward different derivative structures by changing the relative magnitudes of the planar fault energies. These alloying effects are being studied in terms of the structural configuration of dislocations produced, deformation behavior and the resulting ductility of the alloys. A major effort in the first year program was to grow single crystals of the selected alloys and some technical difficulties were encountered. Single crystals of all the selected alloys, with the exception of a tin-containing alloy have now been successfully grown. Tensile testing has been completed for tantalum and titanium-containing alloys. Relative to the binary alloy, the alloying additions were found to significantly increase the critical resolved shear strength CRSS for octahedral slip system without substantially affecting the CRSS for the cube slip system. A possible relationship between ductility of the alloys in polycrystalline form and the relative magnitudes of the CRSS for the two slip systems were discussed. Characterization of dislocations and deformation behavior in selected specimens tested is in progress.

5.0 Future Work

- o Complete tensile testing and deformation analyses of the selected single crystal alloys.
- o Examine critically the relationship between effects of alloying on structural configurations of dislocations, deformation behavior and ductility of the selected alloys.
- o Based on results obtained construct a theory to predict the ductility behavior of Ni_3Al alloys as a function of alloying addition.

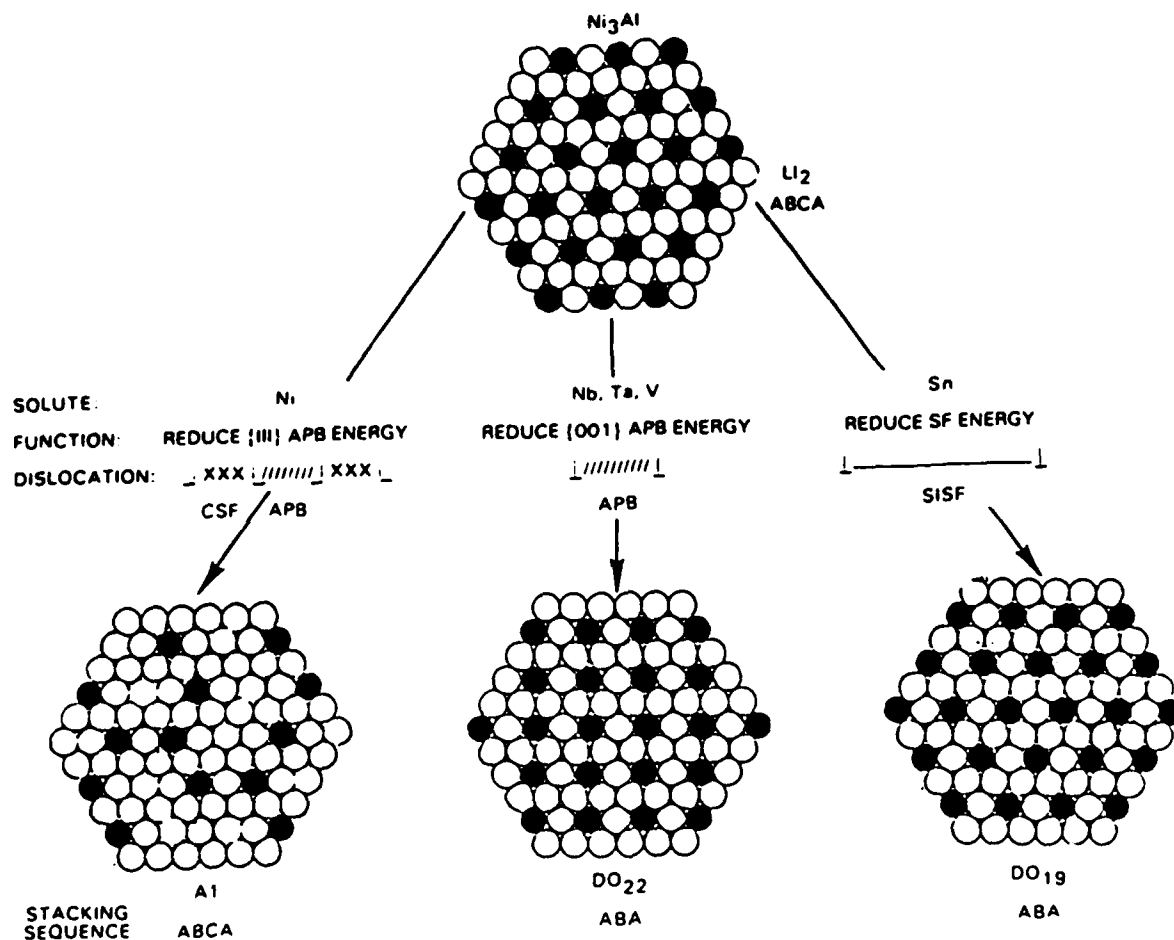


Figure 1 Schematic Diagram Summarizing the Effects of Various Solute Elements on Lattice Stability of the L1₂ Structure and the Likely Types of Dislocation Dissociation Which Would Occur. The Distribution of the Solute Atoms on the Close-Packed Planes of Various Derivative Structures and Their Stacking Sequence are also Depicted

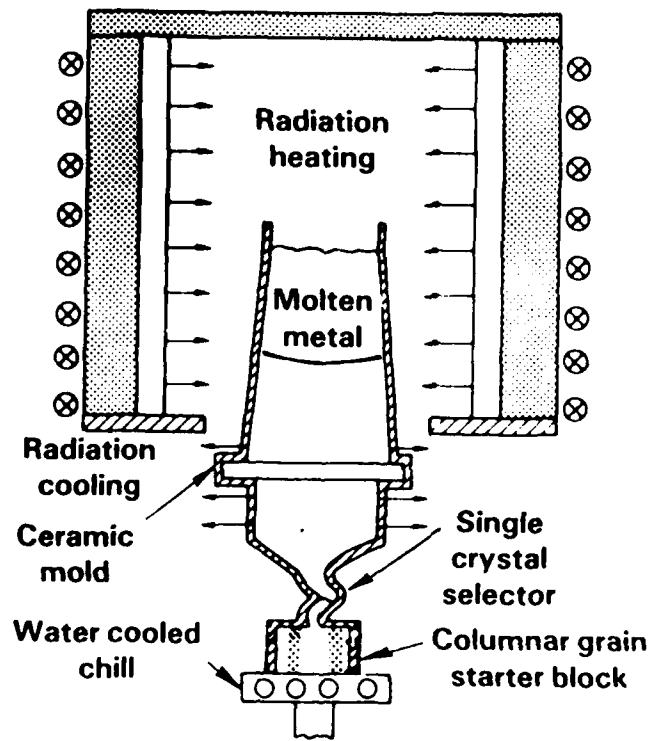


Figure 2 Schematic Drawing of Directional Solidification Process for Growth of Single Crystals

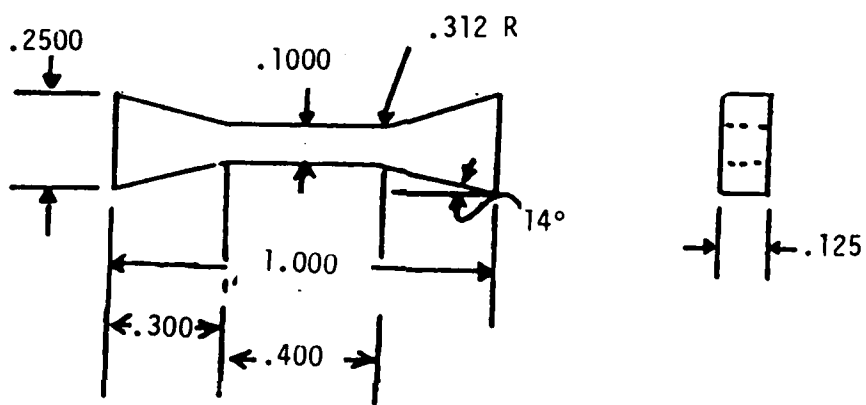


Figure 3 Drawing of Tensile Specimen Used for the Current Studies (Dimensions in Inches)

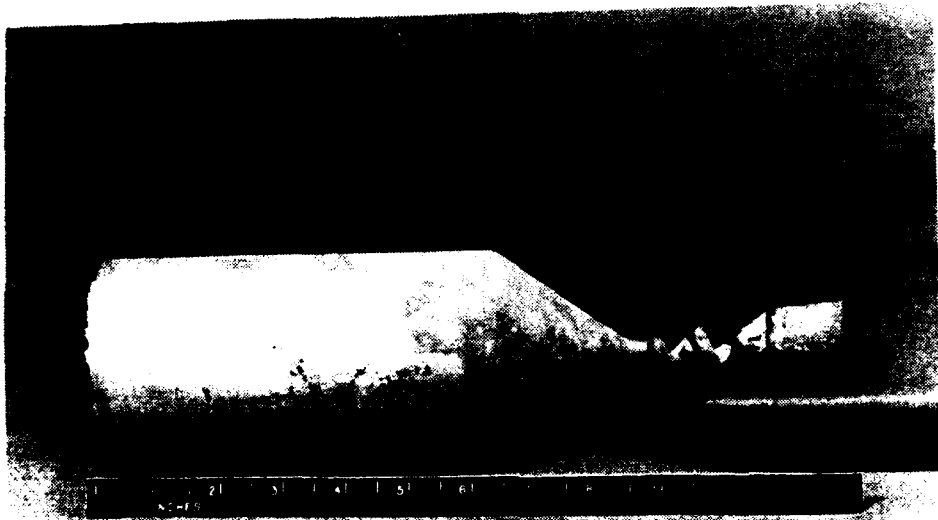


Figure 4 Appearance of a Single Crystal Ingot Removed From the Shell Mold

AL 248
INPUT:

001 210

	TOP		210
0.6	10.7	-20.3	-7.9
-2.2	11.5	15.0	-9.3
-0.6	13.7	17.6	-6.3
-1.4	12.9	17.0	-7.8
1.5	12.1	19.4	-8.4
1.1	15.5	19.7	-4.7
	BOTTOM		
1.0	-11.1	-19.1	7.9
1.0	-10.4	18.7	11.0
1.1	-10.7	18.4	9.9
0.6	-10.7	18.1	10.3
1.4	-10.7	18.7	10.3

ALPHA1 ALPHA2 ALPHA3

11.8 81.6 81.8

MAX ROTATION FROM
AVERAGE ORIENTATION 4.4
INCO01A PAUSE <CR>.....

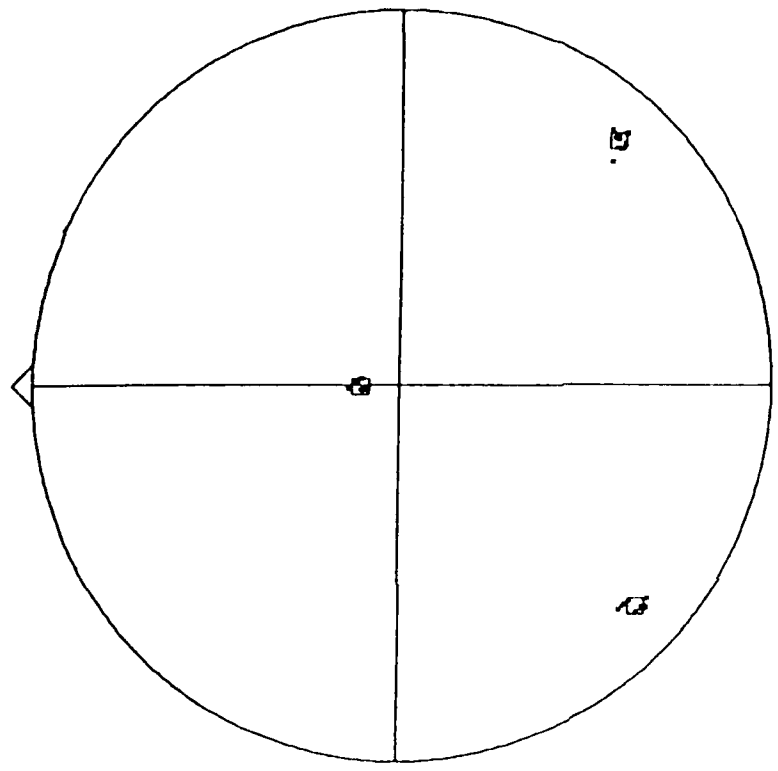


Figure 5 Distribution of <001> Directions on Various Locations on the Top and Bottom Faces of the Single Crystal Ingot of Alloy A1240 With Reference to Three Orthogonal Axes Chosen to be Parallel to the Axis of the Ingot and the Dendrite Arm Directions

TA-195-1
 INPUT:
 001

		210	
	TOP		
-2.3	-7.7	-1.9	19.8
-2.2	-6.6	-1.8	20.5
-2.4	-6.1	-2.3	21.3
-9.2	3.1	18.1	3.4
-8.1	2.8	18.6	3.2
-4.8	2.8	22.9	3.0
4.8	3.9	-22.9	2.4
3.6	3.7	-23.7	2.3
4.8	2.7	-22.1	1.0
-4.7	8.8	-3.2	-17.9
	BOTTOM		
-2.9	-0.6	24.2	-1.0
-3.0	-1.0	-2.7	25.9
-2.7	0.7	24.5	-0.2
-5.7	-1.2	22.2	-1.6
-5.4	-3.2	21.5	-2.5

ALPHA1 ALPHA2 ALPHA3

 2.8 87.4 89.2

MAX. ROTATION FROM
 AVERAGE ORIENTATION: 8.7
 !H001A PAUSE <CR>.....

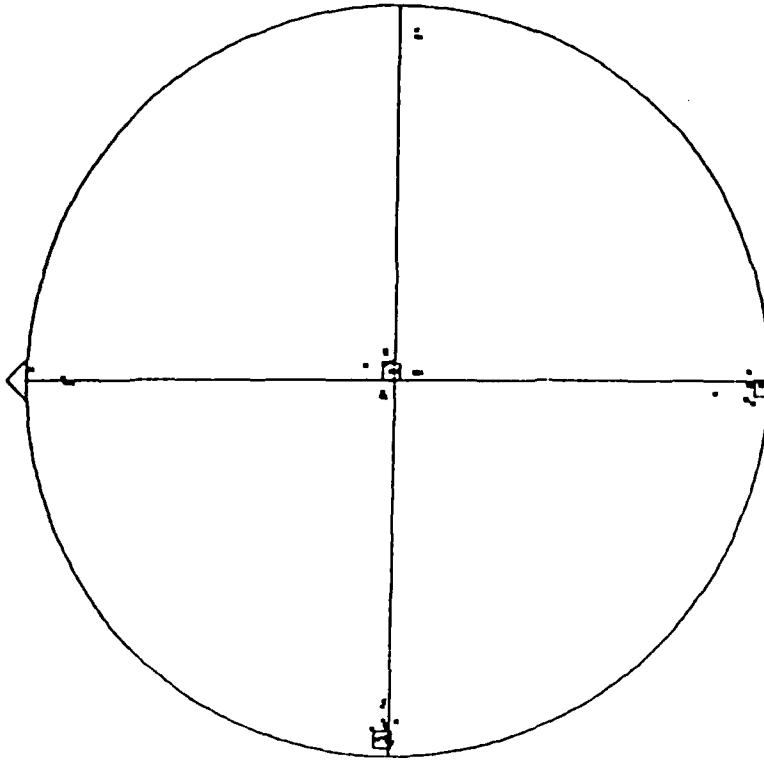


Figure 6 Distribution of <001> Directions on Various Locations on the Top and Bottom Faces of the Single Crystal Ingot of Alloy Ta195 with Reference to Three Orthogonal Axis Chosen to be Parallel to the Axis of the Ingot and the Dendrite Arm Directions



Figure 8 Appearance of a Crystal Section After Cylindrical Slugs with Different Crystallographic Orientations Have Been Removed by EDM Technique

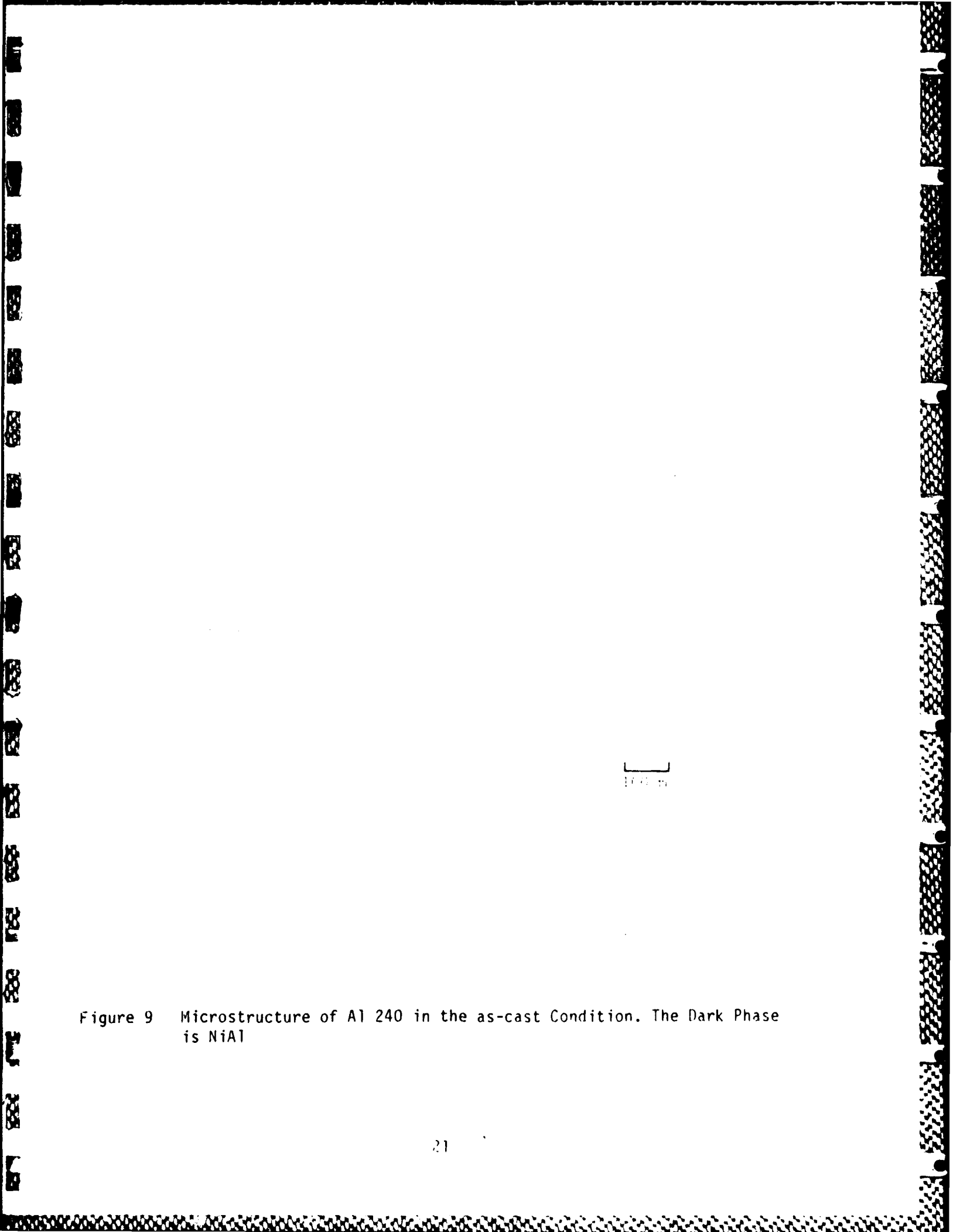
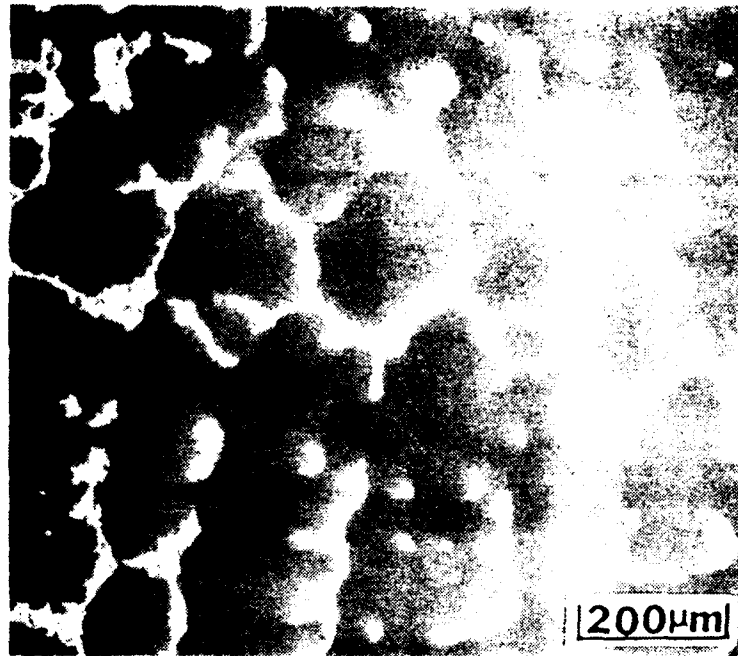
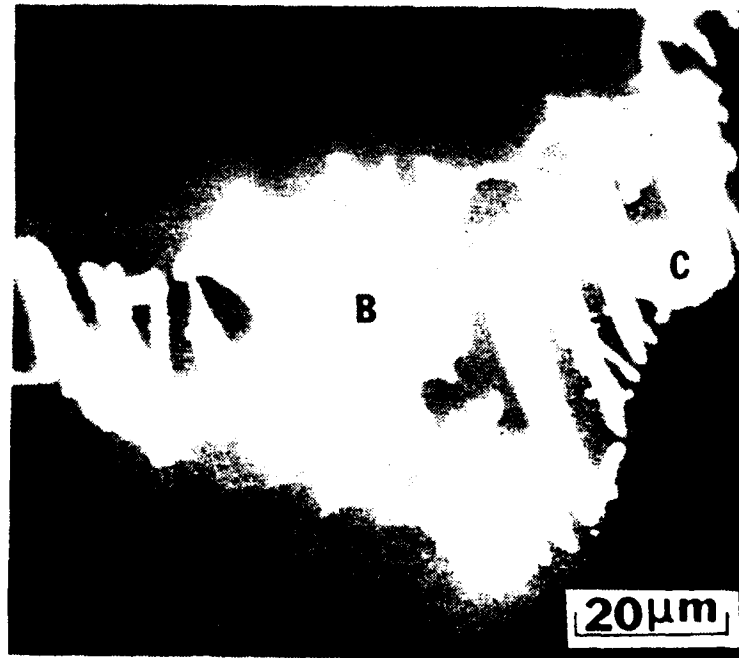


Figure 9 Microstructure of Al 240 in the as-cast Condition. The Dark Phase is NiAl

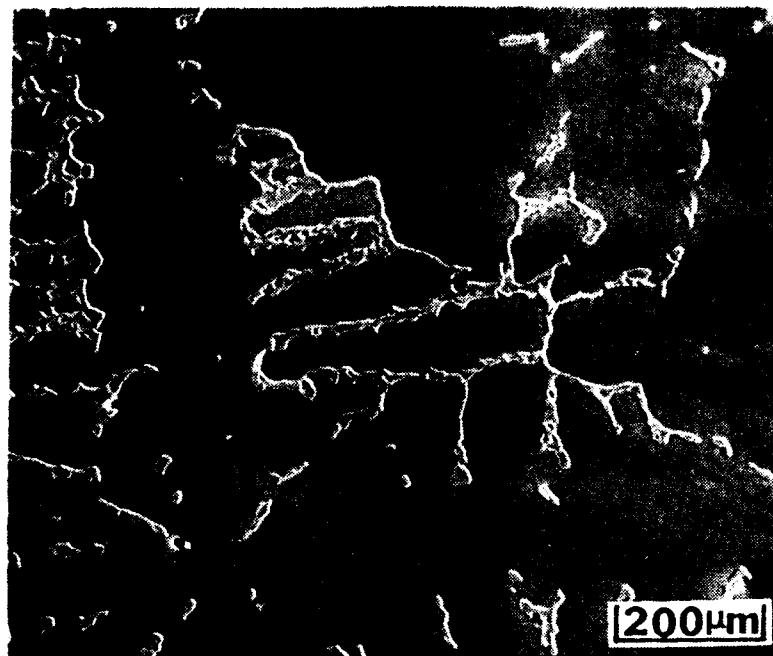


(a)

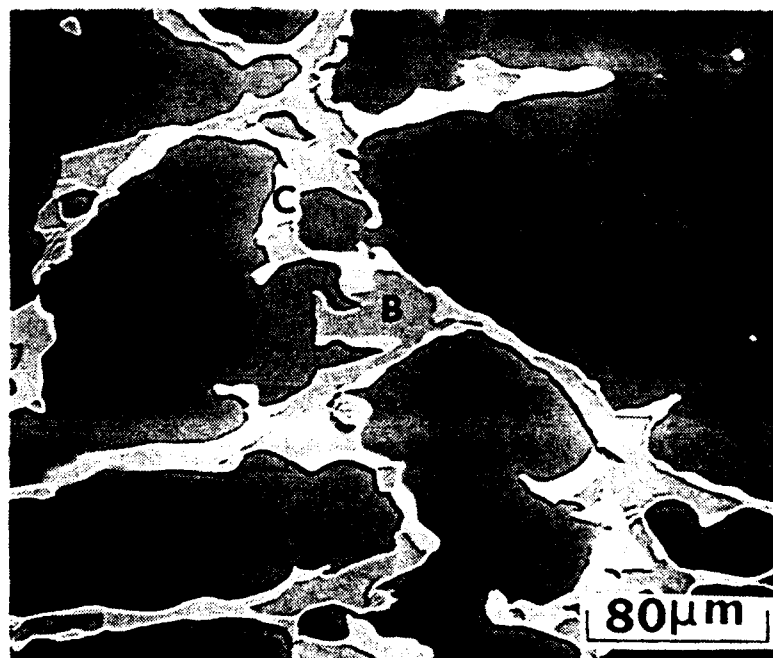


(b)

Figure 10 Scanning Electron Micrograph of Sn 214 in the as-cast Condition. The Compositions of the Phases Labelled A, B and C in (b) are Given in Table 4

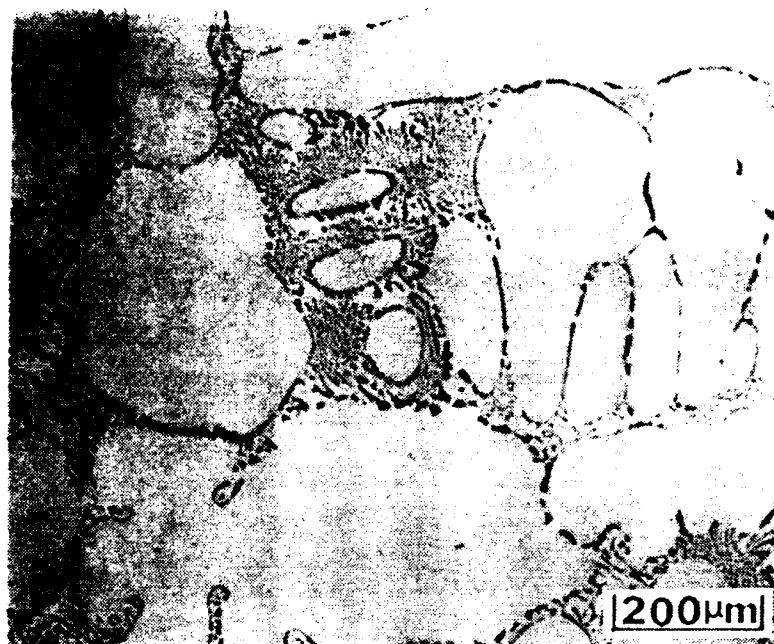


(a)

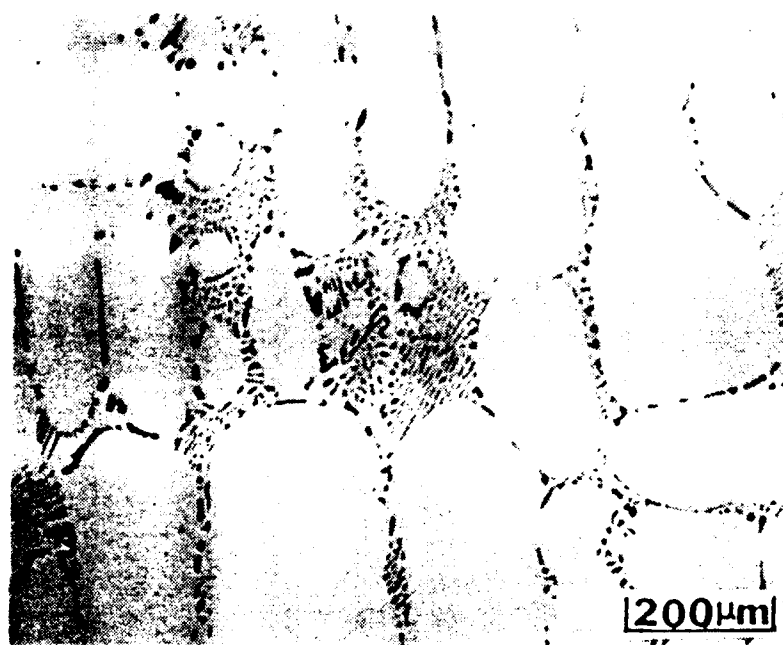


(b)

Figure 11 Scanning Electron Micrograph of Sn 214 After a Heat Treatment of 50 Hours at 1339K. The Composition of the Phases Labelled A, B and C in (b) are Given in Table 4



(a)



(b)

Figure 12 Microstructure of Ta 225 Single Crystal (a) as-cast; (b) After 100 Hours at 1477K. The Dark Phase is NiAl

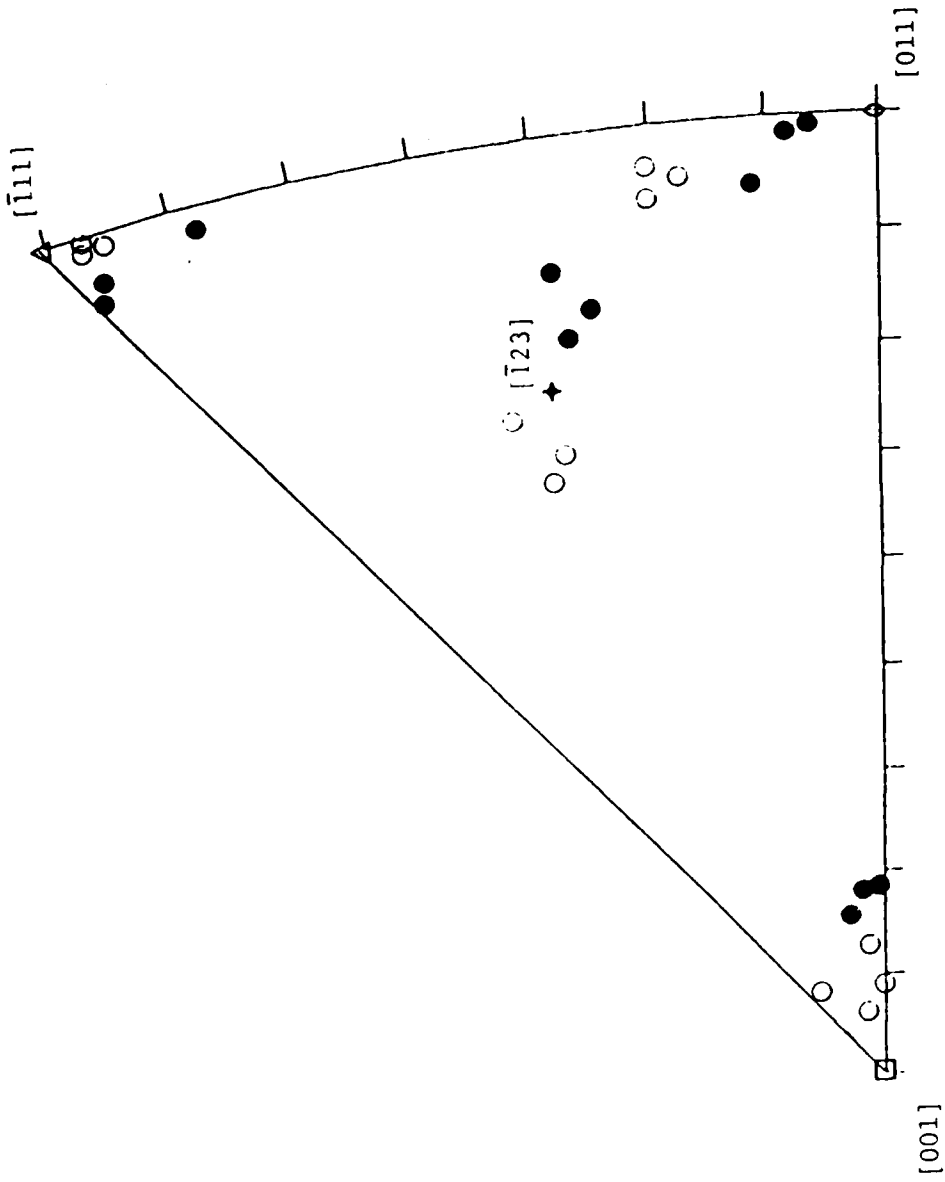


Figure 13 Average of the Actual Orientations for Tensile Specimens of Alloys Ta 195 (●) and Ti 1211 (○)

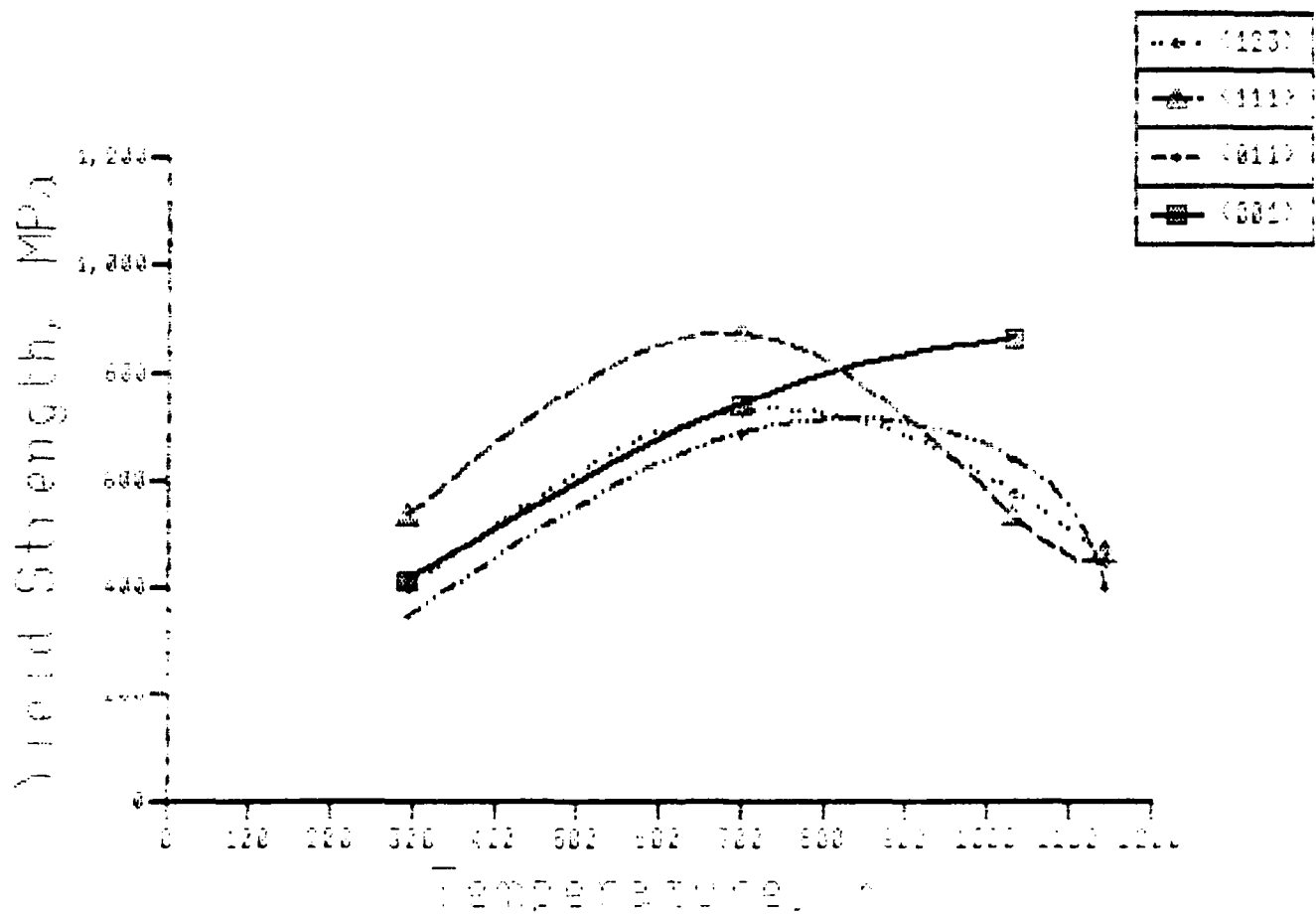


Figure 14 (a) Yield Strength Verses Temperature Curves of Single Crystal Specimens from Alloy Ta 195

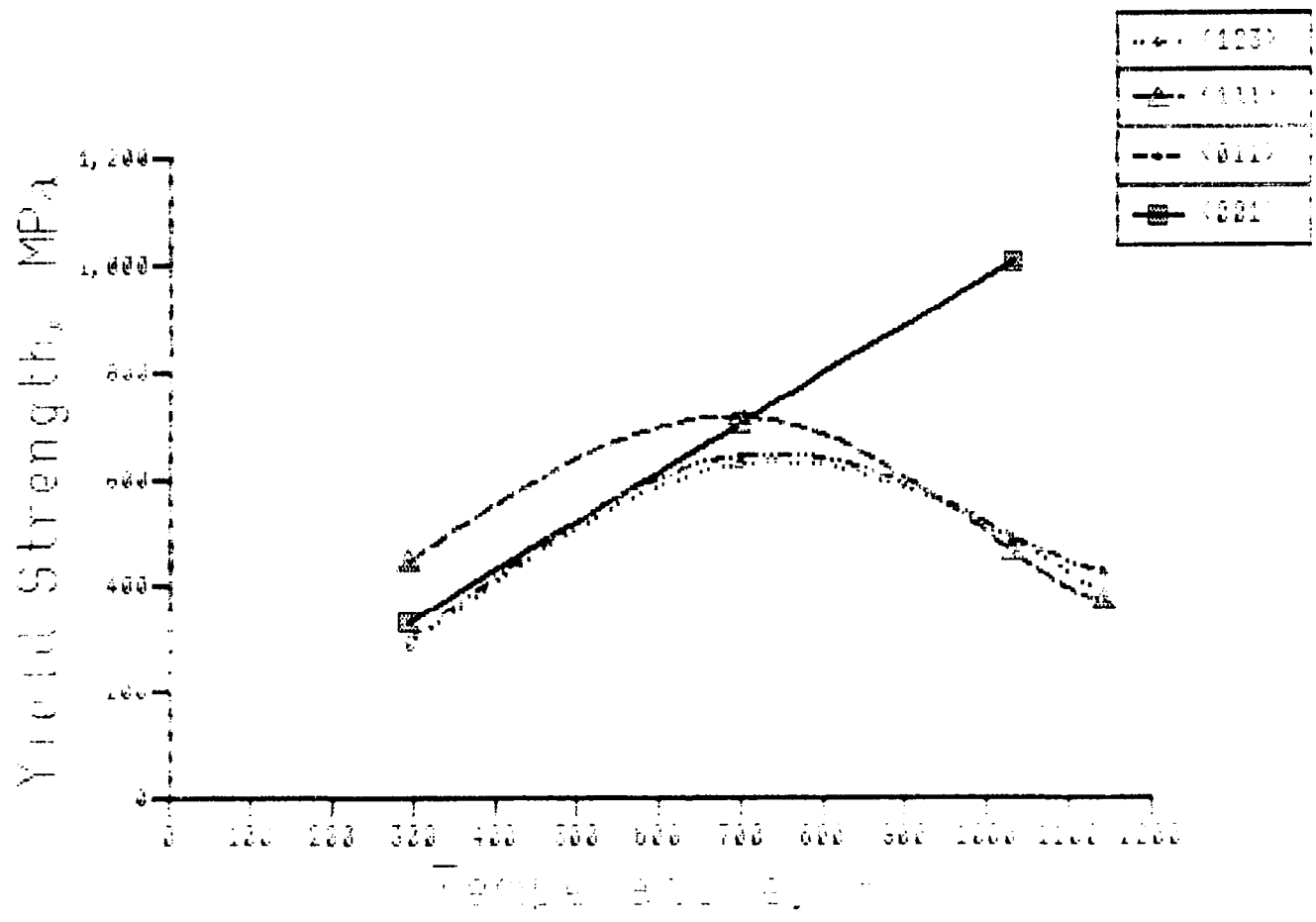


Figure 14 (b) Yield Strength Verses Temperature Curves of Single Crystal Specimens from Alloy Ti 1211

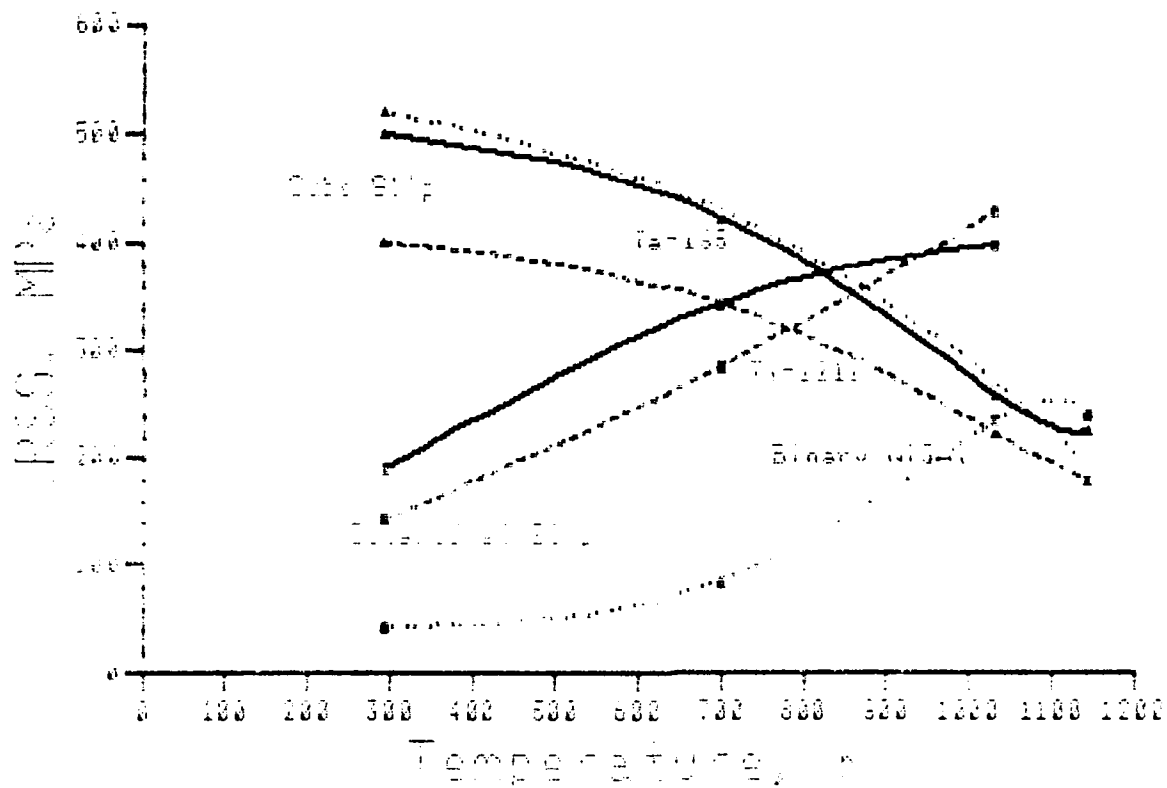


Figure 15 Critical Resolved Shear Strength (CRSS) for Octahedral and Cube Slip Systems in Alloys Ta 195, Ti 1211 and Ni₃Al. The CRSS for Ni₃Al were Calculated from Data of Kear and Copley (Reference 6)

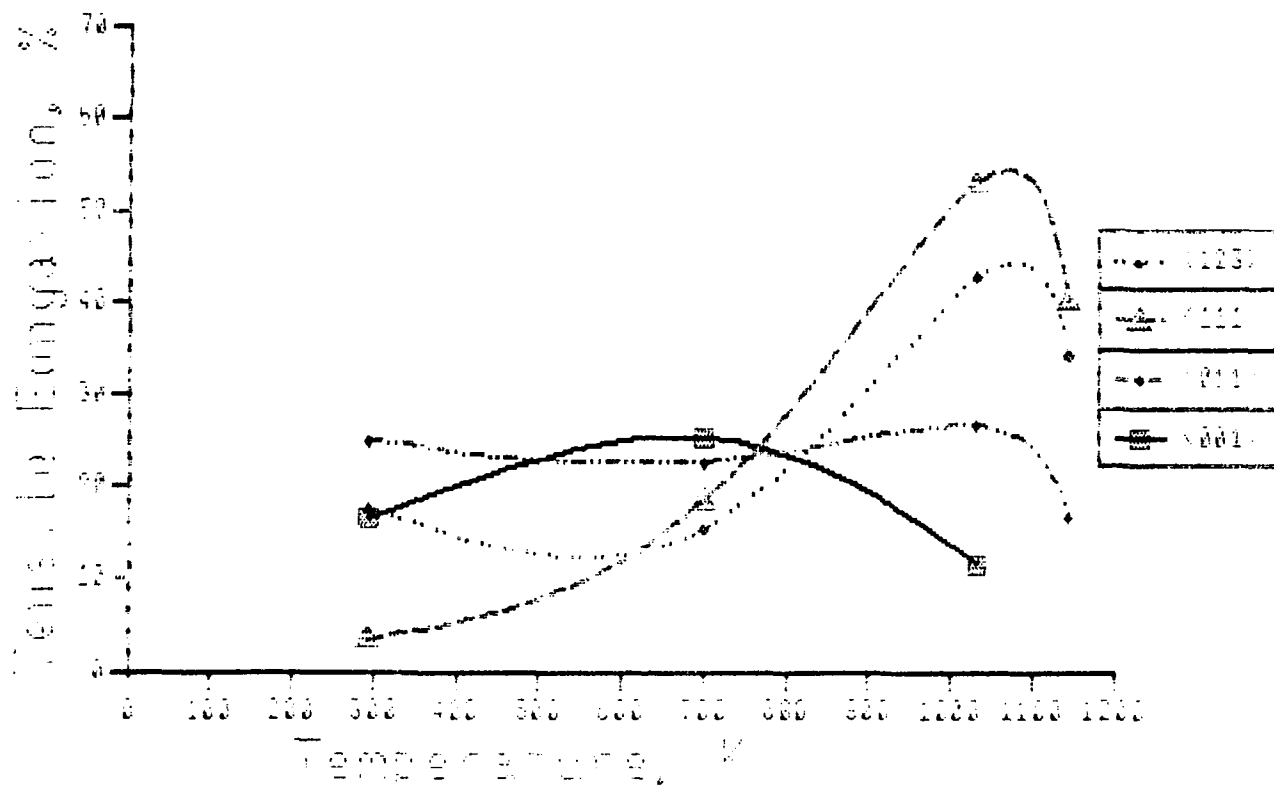


Figure 16 (a) Tensile Elongation Versus Temperature Curves for Alloy Ta 195

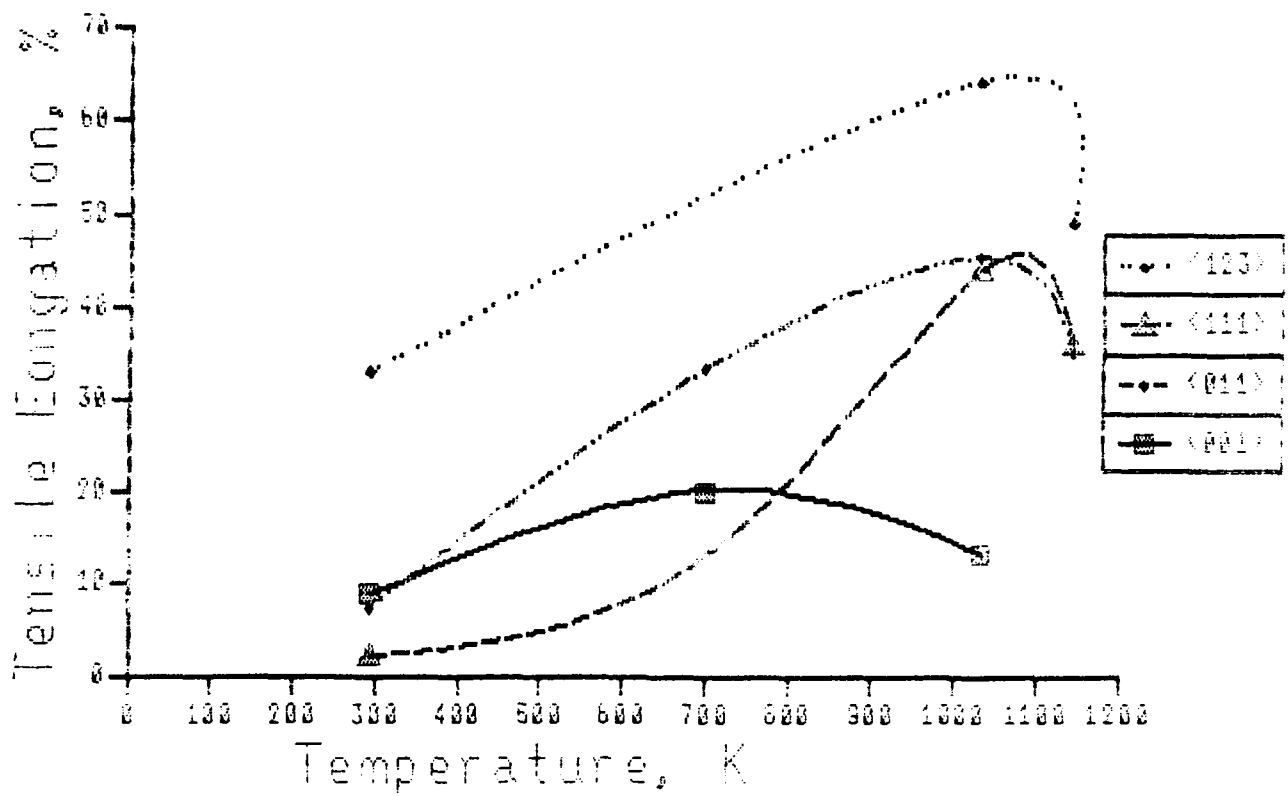


Figure 16 (b) Tensile Elongation Versus Temperature Curves for Alloy Ti 1211

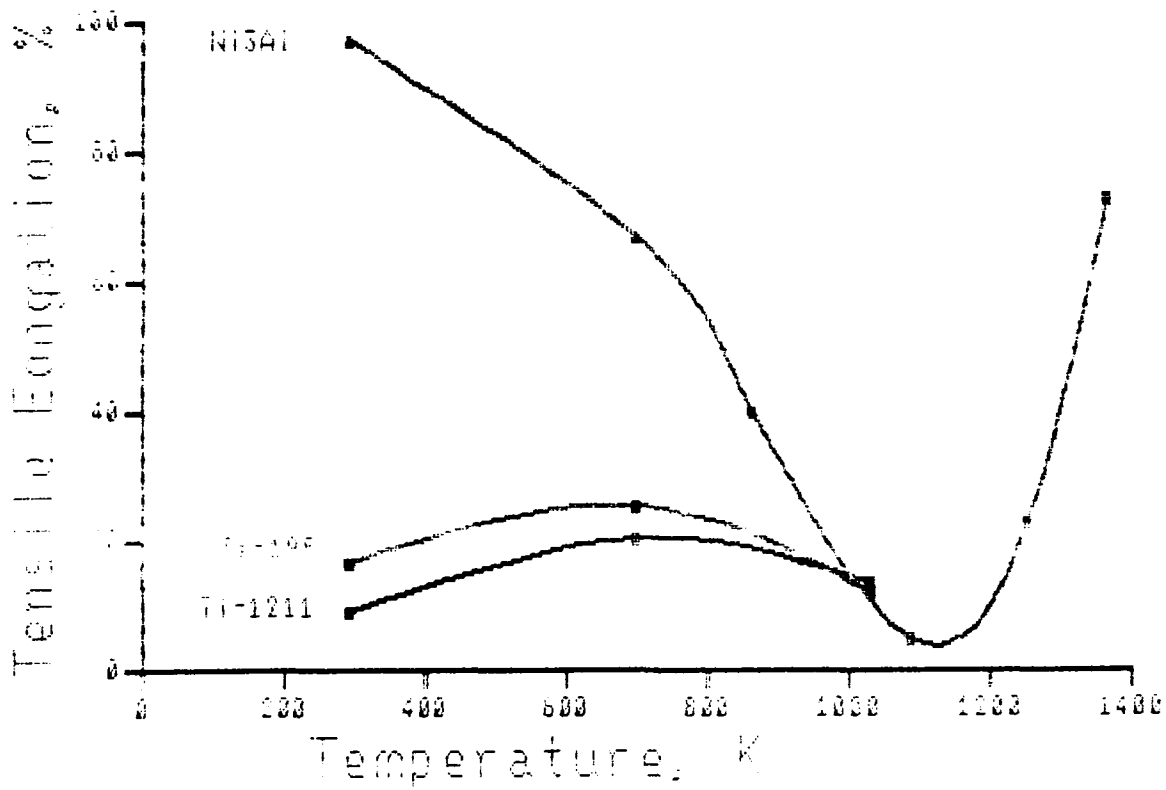


Figure 17 Tensile Elongation Versus Temperature Curves for Alloys Ta 195, Ti 1211 and a Binary Ni₃Al Alloy (Reference 6) in <001> Orientation

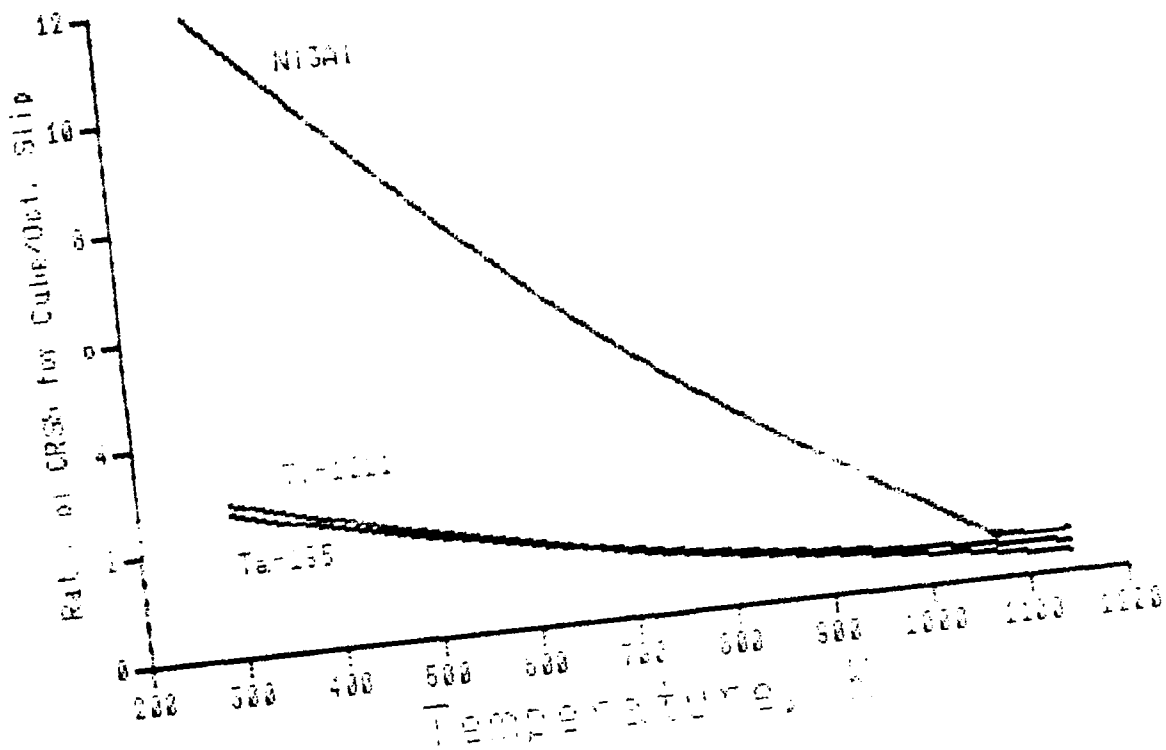


Figure 18 A Comparison of Ratios of Critical Resolved Shear Strengths of Cube Slip to Octahedral Slip in Alloys Ta 195, Ti 1211 and a Binary Ni₃Al Alloy

Table 1

Nominal Compositions of Alloys Selected for Study

<u>Alloy</u>	<u>Atom Percent</u>		
	<u>Ni</u>	<u>Al</u>	<u>Other</u>
Al 240	Bal.	23.5	-
Al 250	Bal.	25.0	-
Al 270	Bal.	26.5	-
Ta 195	Bal.	18.5	5.0 Ta
Ta 205	Bal.	20.0	5.0 Ta
Ta 225	Bal.	21.5	5.0 Ta
Sn 204	Bal.	19.5	4.0 Sn
Sn 214	Bal.	21.0	4.0 Sn
Sn 234	Bal.	22.5	4.0 Sn

Table 2
 Analyzed Alloy Compositions
 Atom Percent

	<u>Ni</u>	<u>Al</u>	<u>Other</u>
Al 240	76.5	23.5	-
Al 250	(1)	(1)	-
Al 270	73.7	26.3	-
Ta 195	76.4	18.6	5.0 Ta
Ta 205	74.7	20.3	5.0 Ta
Ta 225	73.3	21.7	5.0 Ta
Sn 204	75.9	20.1	4.0 Sn
Sn ^r 214	75.8	20.9	3.3 Sn
Sn 234	75.4	21.1	3.5 Sn
Ti 1211	76.9	11.9	11.3 Ti

(1) To be determined.

Table 3

Compositions of the Phases in Al 250 and Al 270

	<u>Ni</u>	<u>Al</u>
Al 250 (Bulk, Nominal)	75	25
Ni_3Al	75.2	24.8
NiAl	64.4	35.6
Al 270 (Bulk, Nominal)	73.5	26.5
Ni_3Al	74.7	25.3
NiAl	62.6	37.4

Table 4
Compositions of the Phases in Sn 214 Single Crystal

	Atom Percent		
	<u>Ni</u>	<u>Al</u>	<u>Sn</u>
As Cast			
Phase A	75.7	23.0	1.2
Phase B	72.8	4.9	22.2
Phase C	60.3	2.4	37.2
After 50 Hours at 1339K			
Phase A	75.0	23.1	1.9
Phase B	73.5	6.5	20.0
Phase C	62.1	4.5	33.4

Table 5

Composition of the Phases in Ta 225 Single Crystal

Phase	Atom Percent		
	Ni	Al	Ta
L1 ₂	73.3	21.1	5.6
B2	60.1	39.9	-

Table-6 Tensile Test Results For Alloy Ta-195 (a) <001> oriented specimens

Temperature Deg. F	K	Spec. Ident.	Axial Orientation		Elong. percent	0.2 % Yield Str		U. T. S.	
			Deg. from <100>	<010>		ksi	MPa	ksi	MPa
		<001>	90	90	0				
70.0	294.1	BA	90.0	81.1	8.9	12.0	57.9	399.2	104.5 720.5
70.0	294.1	CE	89.5	81.2	8.9	21.3	62.1	428.2	101.1 697.1
800.0	699.7	CC	89.5	81.2	8.9	25.4	108.0	744.7	122.1 841.9
800.0	699.7
1400.0	1,033.0	BD	90.0	81.1	8.9	10.6	117.5	810.2	146.3 1008.7
1400.0	1,033.0	CF	89.5	81.2	8.9	13.0	133.2	918.4	152.7 1052.9
1600.0	1,144.1
1600.0	1,144.1

	Schmid Factors		Resolved Shear Strength			
	Octahedral Slip	Cube Slip	Octahedral Slip	Cube Slip	Octahedral Slip	Cube Slip
<001>	0.4084	0.0004	Ksi	MPa	Ksi	MPa
70.0	0.4610	0.1091	26.69	184.04	6.32	43.54
70.0	0.4612	0.1135	28.64	197.47	7.05	48.60
800.0	0.4612	0.1135	49.81	343.43	12.26	84.51
800.0
1400.0	0.4610	0.1091	54.17	373.48	12.82	88.37
1400.0	0.4612	0.1135	61.43	423.56	15.12	104.23
1600.0
1600.0

Table-6 Tensile Test Results For Alloy Ta-195 (b) <011> oriented specimens

Temperature Deg. F	Spec. Ident.	Axial Orientation		Elong. percent	0.2 % Yield St		U. T. S.			
		Deg. from <100>	<010>		ksi	MPa		ksi	MPa	
	<011>	90	45	45						
70.0	294.1	BE	84.5	47.9	42.6	28.2	57.5	396.5	97.9	675.0
70.0	294.1	AB	86.3	45.7	44.6	22.0	42.5	293.0	95.6	659.2
800.0	699.7	BF	84.5	47.9	42.6	21.1	101.8	701.9	115.7	797.8
800.0	699.7	AA	86.3	45.7	44.6	24.6	98.1	676.4	119.1	821.2
1400.0	1,033.0	BC	84.5	47.9	42.6	30.0	98.4	678.5	123.6	852.2
1400.0	1,033.0	AC	86.3	45.7	44.6	23.5	87.5	603.3	120.5	830.8
1600.0	1,144.1	BH	84.5	47.9	42.6	20.1	.	.	100.4	692.3
1600.0	1,144.1	AD	86.3	45.7	44.6	13.7	57.6	397.2	96.9	668.1

Schmid Factors

<011>	Octahedral		Cube
	Slip	Slip	
<011>	0.4085	0.3538	

Resolved Shear Strength

<011>	Octahedral Slip		Cube Slip	
	Ksi	MPa	Ksi	MPa
BE	25.60	176.51	22.94	158.15
AB	18.16	125.18	16.35	112.75
BF	45.32	312.49	40.61	279.99
AA	41.91	288.95	37.75	260.25
BC	43.81	302.06	39.25	270.64
AC	37.38	257.73	33.67	232.13
BH
AD	24.61	169.66	22.16	152.81

Table-6 Tensile Test Results For Alloy Ta-195 (c) <111> oriented specimens

Temperature Deg. F	Spec. Ident.	K	Axial Orientation Deg. from <100>	<010>	<001>	Elong. percent	0.2 % Yield St ksi	MPa	U. T. S. ksi	MPa
	<111>		54.74	54.74	54.74					
70.0	294.1	BE	61.1	52.6	50.9	3.7	91.9	633.7	173.3	1194.9
70.0	294.1	AA	57.0	55.5	51.8	3.4	62.7	432.3	123.2	849.5
800.0	699.7	BH	61.1	52.6	50.9	14.3	130.9	902.6	177.9	1226.6
800.0	699.7	AD	57.0	55.5	51.8	22.8	121.8	839.8	163.0	1123.9
1400.0	1,033.0	BC	61.1	52.6	50.9	45.5	79.8	550.2	109.7	756.4
1400.0	1,033.0	AC	57.0	55.5	51.8	60.7	74.1	510.9	105.3	726.0
1600.0	1,144.1	BF	61.1	52.6	50.9	40.1	66.9	461.3	85.0	586.1
1600.0	1,144.1

	Schmid Factors		Resolved Shear Strength	
	Octahedral Slip	Cube Slip	Octahedral Slip	Cube Slip
<111>	0.2722	0.4715		
70.0	0.3432	0.4863	Ksi	MPa
70.0	0.3036	0.4857	31.54	217.46
800.0	0.3432	0.4863	44.69	308.16
800.0	0.3036	0.4857	19.04	131.26
1400.0	0.3432	0.4863	30.45	209.97
1400.0	0.3036	0.4857	44.92	309.74
1600.0	0.3432	0.4863	63.66	438.93
1600.0	0.3036	0.4857	36.98	254.99
			59.16	407.89
			27.39	188.83
			38.81	267.59
			22.50	155.13
			35.99	248.15
			22.96	158.30
			32.54	224.33
			.	.
			.	.
			.	.

Table-6 Tensile Test Results For Alloy Ta-195 (d) <123> oriented specimens

Temperature Deg. F	Spec. Ident.	K	Axial Orientation Deg. from <100>	<010>	<001>	Elong. percent	0.2 % Yield St ksi	MPa	U. T. S. ksi	MPa
	<123>		74.5	57.69	36.7					
70.0	294.1	AB	75.6	52.6	41.1	15.1	56.1	386.8	102.2	704.7
70.0	294.1	BE	76.1	55.1	38.4	20.3	59.5	410.3	109.1	752.2
800.0	699.7	AC	75.6	52.6	41.1	15.6	100.0	689.5	123.0	848.1
800.0	699.7	BF	76.1	55.1	38.4	15.5	111.9	771.6	136.8	943.2
1400.0	1,033.0	AD	75.6	52.6	41.1	39.0	80.0	551.6	92.7	639.2
1400.0	1,033.0	BG	76.1	55.1	38.4	46.7	87.5	603.3	94.6	652.3
1600.0	1,144.1	AA	75.6	52.6	41.1	23.3	61.8	426.1	77.8	536.4
1600.0	1,144.1	BH	76.1	55.1	38.4	45.3	68.5	472.3	74.7	515.1

Temperature Deg. F	Spec. Ident.	K	Schmid Factors		Resolved Shear Strength					
			Octahedral Slip	Cube Slip	Octahedral Slip	Cube Slip	Ksi	MPa		
	<123>		0.4667	0.4548						
70.0	294.1	AB	0.4554	0.4569	25.55	176.15	25.63	176.74		
70.0	294.1	BE	0.4666	0.4507	27.76	191.43	26.82	184.90		
800.0	699.7	AC	0.4554	0.4569	45.54	313.99	45.69	315.04		
800.0	699.7	BF	0.4666	0.4507	52.22	360.03	50.43	347.74		
1400.0	1033.0	AD	0.4554	0.4569	36.43	251.19	36.55	252.04		
1400.0	1033.0	BG	0.4666	0.4507	40.83	281.52	39.44	271.91		
1600.0	1144.1	AA	0.4554	0.4569	28.14	194.04	28.24	194.70		
1600.0	1144.1	BH	0.4666	0.4507	31.96	220.39	30.87	212.87		

Table-7 Tensile Test Results For Alloy Ti-1211 (b) <011> oriented specimens

Temperature /cu b10	K	Spec. Ident.	Axial Orientation		Elong. percent	0.2 % Yield Str.		U. T. S.		
			Deg. from <100>	<010>		ksi	MPa		ksi	MPa
			<011>		90	45	45			
70.0	294.1	AA	81.3	47.8	43.5	7.5	42.5	293.0	88.8	612.3
800.0	699.7	BF	79.9	47.7	44.1	33.4	93.4	644.0	134.6	928.1
1,400.0	1,033.0	AB	81.3	47.8	43.5	45.4	71.4	492.3	95.2	656.4
1,600.0	1,144.1	AD	81.3	47.8	43.5	35.3	61.9	426.8	78.9	544.0

Schmid Factors

<011>	Octahedral		Cube	
	Slip	Slip	Slip	Slip
	0.4085	0.3538		
70	0.4459	0.4226		
800	0.4436	0.4315		
1,400	0.4459	0.4226		
1,600	0.4459	0.4226		

Resolved Shear Strength

<011>	Octahedral Slip		Cube Slip	
	Ksi	MPa	Ksi	MPa
	18.95	130.67	17.96	123.83
70	41.43	285.65	40.30	277.90
800	31.84	219.53	30.17	208.04
1,400	27.60	190.32	26.16	180.36
1,600				

Table-7 Tensile Test Results For Alloy Ti-1211 (c) <111> oriented specimens

Temperature /cu b10 /cu b10	Spec. Ident.	Axial Orientation Deg. from <100>	Elong. percent	0.2 % Yield Str.		U. T. S.				
				ksi	MPa		ksi	MPa		
	<111>	54.74	54.74	54.74	54.74	<001>				
70.0	294.1	AA	57.6	54.0	52.8	2.2	64.5	444.7	161.0	1,110.1
800.0	699.7	BF	56.6	54.6	53.3	13.2	104.0	717.1	201.7	1,390.7
1,400.0	1,033.0	AB	57.6	54.0	52.8	44.0	66.8	460.6	97.4	671.6
1,600.0	1,144.1	AD	57.6	54.0	52.8	35.9	53.7	370.3	75.5	520.6

	Schmid Factors		Resolved Shear Strength	
	Octahedral Slip	Cube Slip	Octahedral Slip	Cube Slip
<111>	0.2722	0.4715		
70	0.3056	0.4807	Ksi	MPa
800	0.2941	0.4784	19.71	135.92
1,400	0.3056	0.4807	30.58	210.87
1,600	0.3056	0.4807	20.42	140.76
			16.41	113.16
			31.01	213.79
			49.76	343.07
			32.11	221.41
			25.81	177.99

Table-7 Tensile Test Results For Alloy Ti-1211 (d) <123> oriented specimens

Temperature /cu b10	Spec. Ident.	Spec. Axial Orientation Deg. from <100>	Axial Orientation Deg. from <010>	Elong. percent	0.2 % Yield Str. ksi	U. T. S. ksi	MPa	MPa
	<123>	74.5	57.69	36.7				
70.0	294.1	BF	75.4	60.3	33.7	41.6	286.8	88.0 606.8
800.0	699.7
1,400.0	1,033.0	AA	73.2	59.1	36.1	64.3	485.4	86.4 595.7
1,600.0	1,144.1	AB	73.2	59.1	36.1	49.3	375.1	62.0 427.5

	Schmid Factors		Resolved Shear Strength	
	Octahedral Slip	Cube Slip	Octahedral Slip	Cube Slip
<123>	0.4667	0.4548		
70	0.4755	0.4395	Ksi	Ksi
800	0.4625	0.4586	MPa	MPa
1,400	0.4625	0.4586	19.78	136.40
1,600	0.4625	0.4586	32.56	224.49
			25.16	173.47
			32.29	222.62
			24.95	172.02

6.0 References

1. D.P. Pope and S. S. Ezz: *Int. Metals Rev.*, 1984, Vol. 29, No. 3, pp. 136-137.
2. Y. Mishima, Y. Oya and T. Suzuki in *High Temperature Order Intermetallic Alloys Symposium Proceedings*, Materials Research Society 1984 Fall Meeting, Boston, MA.
3. M. Gell, D. N. Duhal, and A. F. Giamei in "Superalloys 1980", *Proceedings of the Fourth International Symposium on Superalloys*, September 1980, Ed. J. K. Tien, S. T. Wlodek, H. Morrow III, M. Gell, and G. E. Mauer, ASM Publication, pp. 205-214.
4. D. Dimiduk, AFWAL/MLLM Wright-Patterson AFB, Ohio 45433-6533, Private communication, March 1987.
5. C. Lall, S. Chin and D. P. Pope: *Metall. Trans. A*, 1979, Vol. 10A, pp. 1323-1332.
6. S. M. Copley and B. H. Kear: *Trans. TMS-AIME*, 1967, Vol. 239, pp 977-984.
7. D. M. Wee, D. P. Pope and V. Vitek: *Acta Metall.*, 1984, Vol. 32, No. 6, pp 829-836.
8. C. C. Law and M. J. Blackburn: "Rapidly Solidified Alloys for Disk Applications" Air Force Contract No. F33615-83-C-5103, Final Report, 1987 (to be published).

ENO

7-87

DTIC